
Mechanical Processing in the ICE Model

Anupam Prasad Vedurmudi



München 2013

Mechanical Processing in the ICE Model

Anupam Prasad Vedurmudi

Dissertation
an der Fakultät für Physik
der Ludwig-Maximilians-Universität
München

vorgelegt von
Anupam Prasad Vedurmudi
aus Kolkata, Indien

München, den June 18, 2013

Erstgutachter: Prof. Dr. J. Leo van Hemmen

Zweitgutachter: Zweitgutachter

Tag der mündlichen Prüfung: Prüfungsdatum

Contents

Abstract	xi
1 Introduction	1
1.1 Mechanical Processing of Auditory Stimuli	2
1.2 Pressure Difference Ears - The ICE Model	2
2 The ICE Model	5
2.1 Description of the Model	6
2.1.1 Mouth Cavity	6
2.1.2 Middle Ear System	7
2.1.3 Head Model and External Sound Input	10
2.2 Derivation of the Model	11
2.2.1 Internal Cavity	14
2.2.2 Vibration of the Membrane	17
2.2.3 Vibration of Coupled Membranes	21
2.2.4 Circuit Model	27
3 Evaluation of the Model	29
3.1 Sound Localization Using the ICE-Model	30
3.1.1 Membrane Vibration Velocity	31
3.1.2 Directional Hearing Cues	34
3.1.3 Parameter Estimation	37
3.2 Spatial Vibration Pattern of the Membrane	39
4 Conclusion	43
Acknowledgements	47

List of Figures

1.1 Vertebrate Ear Evolution	3
1.2 Cross Section of a Lizards Head	4
2.1 Illustration of a gecko's head	5
2.2 Previous and current ICE model representations	8
2.3 Extracolumella Flection	9
2.4 Tympanic membrane model	10
2.5 Previous acoustic head model for geckos	12
2.6 New acoustic head model for geckos	13
2.7 Circular membrane eigenmodes	19
2.8 Sectoral membrane eigenmodes	22
2.9 Low frequency circuit analog	27
3.1 Vibration amplitude for the common house gecko	32
3.2 Vibration amplitude for the Tokay gecko	32
3.3 Frequency dependence of ipsi- and contralateral membrane vibration amplitudes - common house gecko	33
3.4 Frequency dependence of ipsi- and contralateral membrane vibration amplitudes - Tokay gecko	34
3.5 Frequency dependence of membrane vibration amplitudes for different directions.	34
3.6 Direction dependence of membrane vibration amplitudes for different frequencies.	35
3.7 ILD plots for the common house gecko	37
3.8 ILD plots for the Tokay gecko	38
3.9 Direction dependence of the Interaural Level Difference for different frequencies.	39
3.10 Tympanic membrane vibration profiles for the Tokay gecko.	40

List of Tables

2.1	Functions and Parameters used in the ICE Model	13
2.2	Functions and Parameters used in the ICE Model contd.	14
3.1	ICE Model geometry Parameters for the common house gecko (<i>Hemidactylus frenatus</i>) and the Tokay gecko.	30

Abstract

Hier steht eine maximal einseitige Zusammenfassung der Dissertation.

Dies ist ein neuer Absatz.

Chapter 1

Introduction

The auditory system is among the most ubiquitous of sensory systems as evidenced by the development of numerous strategies for the detection and processing of auditory stimuli across several species. The processing of sound stimuli is fairly fast and in comparison to light stimuli, sound has two main properties - it is omnidirectional and due to its large wavelength, it isn't blocked by small objects. For instance we can hear objects behind us or behind obstacles whereas the same isn't true for visual stimuli. These properties give the animal the obvious advantage of being able to react to approaching dangers that aren't yet visible. In order to fully utilize the sound stimuli, it is therefore essential that an animal is able to assess the direction or, to use the technical term, *localize* a sound source.

Before we discuss the various sound localization methods observed in nature, we first go through the fundamental steps involved in auditory perception. First, an object generates an auditory stimulus which in general can be very complex. This stimulus then propagates through a given medium (e.g. air, water) and excites the primary receiver(s) of the animal. In most terrestrial vertebrates, these take the form of *tympani* or eardrums - a pair of thin vibrating membranes which are a component of the mechanical part of the auditory system. Depending on the species, there may be an apparatus that focuses and amplifies the sound waves. In humans for example, this function performed by the external ears or pinnae. The vibrations are then transmitted by means of a set of bony or cartilaginous elements and converted into electrochemical signals that will be processed neuronally; see Sec. 1.1.

The neuronal processing system consists of building blocks called *neurons* which are connected to each other through *synapses*. The entire system is referred to as a *neuronal net* which, through a form of computation, gives rise to representations of the stimuli known as *neuronal maps*. Each neuron of the map represents a specific property, e.g. the position in space or the frequency of the stimulus and neighbouring neurons respond to similar sensory inputs. Neuronal maps serve to reconstruct stimuli as optimally as possible within the limits of processing. The precise calibration of the synapses required for stimulus reconstruction is a result of experience-based learning processes that take into account inputs from all available sensory systems.

The primary focus of this thesis is the mechanical processing that is responsible for the sound localization ability of certain terrestrial vertebrates. Specifically, we are interested

in the analytical treatment of hearing in animals that have their eardrums connected through a large mouth cavity and the enhancement of directionality in the response of such systems; see Sec. 1.2. Although our model can be scaled to several different species, for the purposes of a thorough comparison, we will be putting a special emphasis on lizard hearing. The questions posed by the neuronal processing of auditory stimuli in these animals although interesting, are beyond the scope of this thesis.

1.1 Mechanical Processing of Auditory Stimuli

Ancestors of most modern vertebrates including frogs, turtles, lizards, birds, crocodilians and mammals developed a pair of tympani (thin vibrating membranes) to detect incoming sound waves and transmit them from the air to the ossicles in the middle ear; cf. Fig. 1.1. Despite the large variation in size and shape, two groups with fundamentally distinct constructions can be made out. Mammals possess tympani that are effectively separated from and therefore acoustically independent of each other. In contrast, the other group consisting of reptiles (lizards, turtles, crocodiles), birds and frogs have Internally Coupled Ears (for reviews see [1], [2] and [3]) wherein the tympani are connected through large Eustachian tubes as illustrated in 1.2. The evolutionary appearance of independent and coupled ears (Fig. 1.1) suggests that the latter are probably early tympanic ears.

1.2 Pressure Difference Ears - The ICE Model

The ability of humans and most other mammals to localize sources of sound depends on two kinds of information: the direction and frequency of the source may cause differences between the amplitudes and arrival times of sounds reaching both ears. These pieces of information are referred to binaural hearing cues or simply hearing cues. In mammals there is an additional source of directionality due to the shape of the pinnae which affects the spectra of sounds reaching the ear. However, most hearing animals are lack monoaural cues and the binaural cues are at best too small to affect the neural responses of the ears, [5]. These animals are in general too small in comparison to the wavelength of sound in their typical hearing range to cause an appreciable amplitude differences due to diffraction. Nevertheless, the eardrum vibration amplitude has been found to vary strongly with direction. In order to resolve this apparent paradox it was suggested by Autrum [6] that the directionality could be a result of the ears vibrating due to the differences between the pressure on the inner and outer surfaces (see [7] for a review). The properties of such systems were also found to be analogous with the inherently directional nature of pressure gradient receivers studied by Harry Olson ([8]). Pressure difference reception has become the standard explanation for directionality in almost all small animals; the one exception being mechanically coupled eardrums in some parasitic flies, (see Robert *et al* [9]).

The pathway for sound to the inner surface of the eardrum varies. In many animals the air spaces behind the eardrums are connected by sizable air-filled passage which results

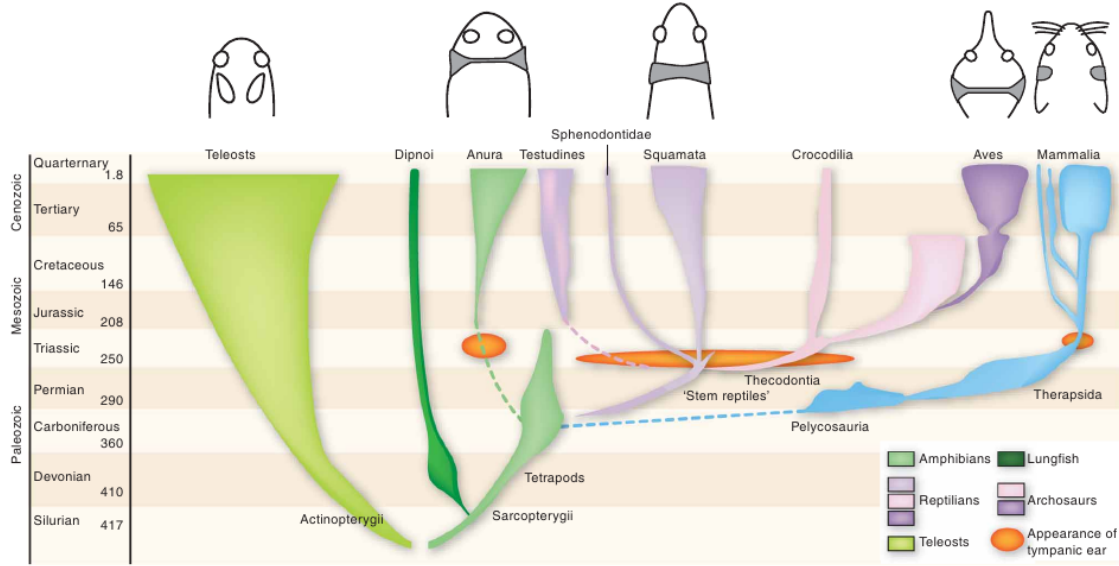


Figure 1.1: Evolution of vertebrate ears. Tympanic middle capable of receiving airborne sound evolved independently among the ancestors of modern frogs, turtles, lizards, birds, crocodilians and mammals. Diagrams at the top show cross-sections through different heads of these animals (middle ears - gray fill). Among these middle-ear systems two distinct groups can be observed - the anura (frogs and toads), squamata (lizards and snakes) and aves (birds) form one group with ears connected through differently shaped cavities and mammals with independent ears. Figure due to Schnupp and Carr [3].

in a coupling between the eardrums. This has been shown for insects ([10]), frogs ([11]) and reptiles ([4]). The sound wave may alternatively reach the inner surface of the eardrum through a different route (like the tracheal tube in crickets). Our focus is on the former type of animals, i.e. animals that have their eardrums coupled through an air-filled cavity.

Our study will take place in two main steps. In Chapter 2 we will present our model for the mechanical processing of auditory signals in systems with internally coupled ears - the ICE Model. Since our focus is on an analytical model, we would like to have a system that reduces to tractable mathematical expressions so that we can clearly see the dependence of the system's behaviour on its parameters. To this end we will model the combination of the eustachian tubes, middle ear cavity and pharynx as a single continuous cylindrically shaped air cavity; see Sec. 2.1.1. The ears will be modelled as linear elastic membranes that are circular with an omitted sector that corresponds to the extracolumella - the extension of the columella that is in contact with the ear. The sound inputs to both the ears will be modelled as pressure waves of a given frequency with a phase difference that depends on the head size. The aim of the chapter is to find expressions for the quantities which give us the directional output of the system.

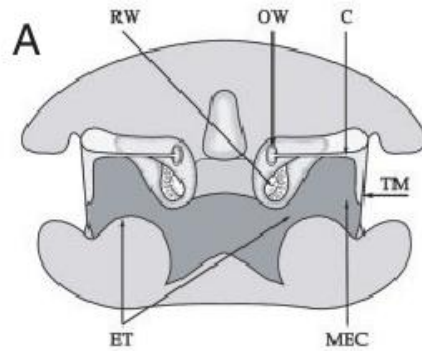


Figure 1.2: Diagram of the cross-section of a lizards head (*sceloporus*). The Tympanic Membranes (TM) as well as the air inside the Middle Ear Cavity (MEC) and Eustachian Tubes (ET) are excited by incoming sound waves. Due to the considerable width of the Eustachian Tubes (ET), the air inside the Pharynx (P) is excited as well. The vibration of the tympanum causes a movement of the attached middle ear, Columella (C) whose lever construction transmits the vibrations to the Oval Window (OW), the membrane at the entrance of the fluid filled cochlea. Figure taken from [4]. The vibration of the OW excites the fluid in the Cochlea which gives rise to a frequency-dependent activation of the embedded basilar membrane and underlying auditory nerve fibers. The Round Window (RW) is a membrane at the end of the cochlea that serves to compensate the pressure within the fluid.

In Chapter 3 will evaluate the validity of our model by comparing the calculated values of the membrane vibration velocity with experimentally determined quantities; see 3.1.1. In addition to testing the directional frequency response of the system we will also define quantities that could serve as directional cues. These two quantities are known as the iTD (*Internal Time Difference*) which measures the delay between the membrane vibrations and the iLD (*Internal Level Difference*) which measures the difference in their vibration amplitudes; Sec. 3.1.2. These quantities are defined in contrast to the *Interaural* Time and Level Differences which serve as directional cues in the absence of coupling. Due to the difficulty of measurement of certain membrane properties (e.g. fundamental frequency, damping coefficients), in Sec. 3.1.3 we will also provide means of estimating these quantities from observations. In the final section of this chapter, Sec. 3.2, we will compare the vibration profile of our model tympanum with that of a realistic tympanum and thereby seek to explain the complex patterns of the observed.

Chapter 2

The ICE Model

Several terrestrial vertebrates, e.g. lizards, frogs, alligators and many birds, possess a hearing mechanism very different to that of mammals: their tympanic membranes are coupled through large eustachian tubes and a large mouth cavity resulting in the influence of the vibrations of one tympanic membrane on those of the other. This is illustrated in 2.1. The typically small head sizes (compared to sound wavelength) of these animals result in small phase differences (ITDs) and negligible amplitude difference (ILDs) between the ears. The coupling serves to enhance the ITDs and create ILDs between the tympanal vibrations. These differences show directionality and serve as hearing cues for localization.

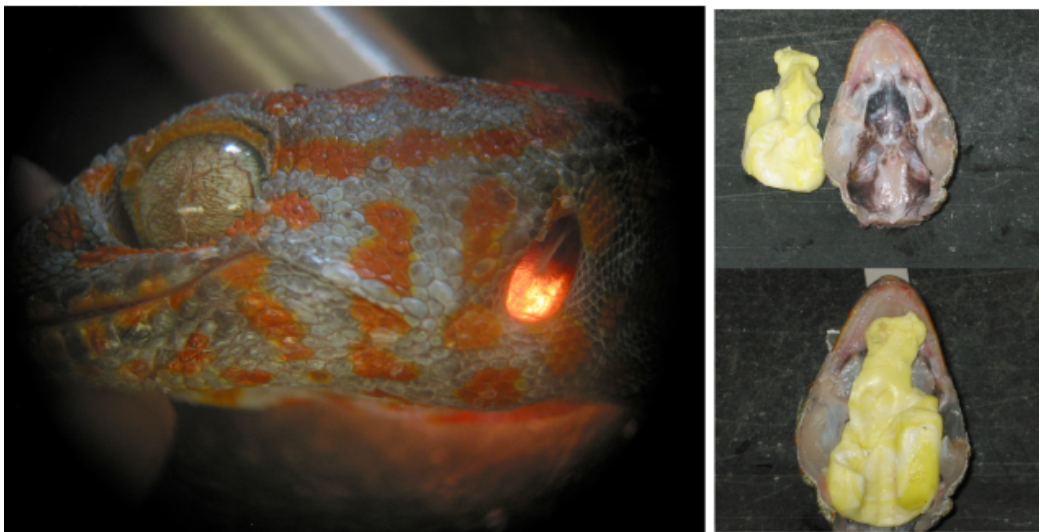


Figure 2.1: Left: Picture of a Tokay gecko's head with the snout pointing to the left. The tympanic membrane is illuminated from behind by a light source on the other side of the head. The cartilaginous extracolumella can be seen attached to the upper part of the membrane. Right: Cast imprint of the mouth cavity of the gecko with the snout pointing to the top. The figures illustrate the coupling of the tympani through the mouth cavity. Photographs courtesy of Jakob Christensen-Dalsgaard.

Proceeding from the earlier work done by Vossen in [12] and [13], in this chapter we present a model for such a system of coupled ears with an emphasis on lizard hearing - specifically the Tokay gecko and the common house gecko. Our goal is to demonstrate its main aspect of such a system - the coupling of the eardrums through the mouth cavity. The main components of such a system are the mouth-cavity, the two tympani and the two *extracolumella* (one on each tympanum). In general, the shape of the mouth-cavity is highly irregular and therefore not conducive to an analytical treatment. Moreover, the system corresponds to a pair of coupled second-order PDE's with moving boundaries. For this reason we will need to make further approximations in order to facilitate an analytic solution.

In order to make the system more analytically tractable we will, as before, study a geometry in which a pair of rigidly clamped linear elastic membranes are coupled through a cylindrical cavity. The cylindrical geometry allows an accurate calculation of the pressure distribution inside the cavity at both low and high frequencies. By accounting for the presence of the asymmetrically attached extracolumella, we will also explain the complex vibration patterns of the membrane. We will conclude this chapter with a comparison of our model with previous methods that have used a electrical circuit analogy to model the system. At the end of this chapter, we will have the expressions that describe the steady-state vibrations of both eardrums as a function pressure amplitude, direction and frequency.

2.1 Description of the Model

Before heading to a quantitative analysis of the ICE model, we will first need to list its basic components. and justify their properties based on realistic anatomical properties of the vertebrates in question. Our emphasis is on an analytical treatment of the ICE model. In Sec. 2.1.1, we will describe the cylindrical model for the mouth cavity and state the reasons for our choice of the geometry and the dimensions used. We will then proceed to describe the middle ear system and its main components of interest, the *extracolumella* and the *tympani* in Sec. 2.1.2. Finally, in Sec. 2.1.3 we will analyse the dependence of the acoustic input to both eardrums on the direction of the sound source, head size and shape.

2.1.1 Mouth Cavity

In the earlier treatment of the ICE model, the mouth cavity is modelled as a simple cylinder closed at both ends by rigidly clamped (baffled) circular membranes; these model the tympanic membranes. As shown by Vossen in [12, p. 21] and [13], the length of the cylinder was chosen to be equal to the interaural distance and the radius of the model tympanum is determined from the typical area of the realistic tympanum. The advantage of using a cylindrical cavity model for the mouth cavity is that the pressure distribution inside the cavity is easy to calculate. The pressure distribution inside the cavity becomes highly

non-uniform with increasing frequency and a cylindrical cavity simplifies its calculation¹.

On the other hand, in this description the small area of the tympani results in a cavity volume which is an order of magnitude smaller than that of the realistic mouth-cavity in the corresponding animal. In general, a smaller volume results in a stronger coupling between the tympani. The exact nature of this coupling will be discussed in the next chapter when we perform a thorough evaluation of the complete system.

In order to get around this problem we make some slight modifications to the model. Essentially, we maintain the cylindrical shape of the internal cavity but require it to have a volume which is equal to that of the realistic cavities in typical specimens. This volume is denoted by V_{cav} . While maintaining the same tympanum size and interaural distance we can therefore calculate the radius of the cylinder as,

$$a_{cyl} = \sqrt{\frac{V_{cav}}{\pi L}} \quad (2.1)$$

where a_{cyl} is the cylinder radius and L is the interaural distance. Simply put, the model consists of a cylindrical shell of radius a_{cyl} and length L with circular holes on either side with the radius of the tympanic membrane, a_{tym} . These holes are in turn closed by rigidly clamped membranes which will be described in the next section. The previous and current geometric representations of our model are shown in figures 2.2a and 2.2b. The darkly shaded circular surfaces in fig. 2.2b at ends 0 and L correspond to the two eardrums.

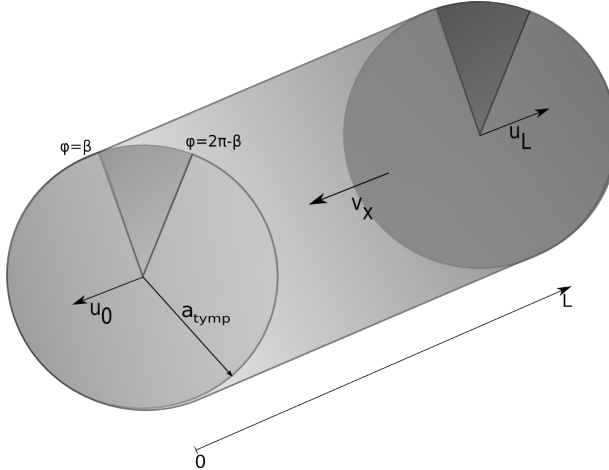
We will be working with the cylindrical polar coordinates, (r, ϕ, x) . The direction along the cylindrical axis is denoted by x and (r, ϕ) are the polar coordinates of the plane perpendicular to the x -direction. Directions outward from the cylinder are taken as positive (in x) and those inward are taken as negative.

2.1.2 Middle Ear System

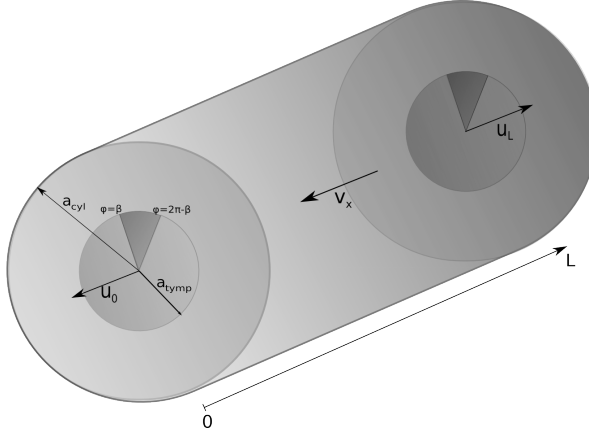
The main components of the middle-ear of lizards are the two eardrums, the columella and the two cartileginous extracolumella. The tympanic membrane or the eardrum is a thin membrane that separates the outer ear and the middle ear and vibrates in response to external sound waves. Unlike humans, lizards possess only a single middle ear bone, the *columella*, that is connected to both eardrums by means of a cartileginous element, the *extracolumella*.

The membrane-extracolumella-columella system functions as a second-order lever where the membrane - driven by the internal and external pressures - causes a displacement of the extension of the extracolumella (known as the inferior process). This motion is in turn transmitted via the columella and columellar footplate to the inner ear (cochlea). The inner-ear translates this motion into electrochemical impulses which will be passed on to the brain via the auditory nerve; cf. Fig. 1.2. The columella-extracolumella system

¹We are in effect modelling the combination of the middle ear cavity, pharynx and eustachian tubes as a single continuous cavity. This is a reasonable approximation due to wide eustachian tubes typically seen in lizards.



(a) The previous geometric representation of the ICE model.



(b) The representation of the new model.

Figure 2.2: The bold arrows represent the direction conventions along the cylinder's axis. The new model is represented by a cylinder of radius a_{cyl} and length L closed at both ends by sectoral membranes of radius a_{tymp} . The darkly shaded region corresponds to the extracolumella; see Sec. 2.1.2.

effectively transmits the mechanical vibrations from the eardrums to the inner ear. In the human middle-ear, the same function is performed by the bones *malleus*, *incus* and *stapes*, which are collectively known as the ossicles.

For low frequencies (below 4kHz), the extracolumella (or more accurately, the inferior process of the extracolumella) moves as a completely stiff bar. It was shown by Manley [14] that the extracolumella begins to flex at higher frequencies - this is illustrated in fig. 2.3. This is partly responsible for the poor high-frequency response of gecko middle ears - a feature also observed in other non-mammalian vertebrates. The reason for this is that, due to the flexion some energy is lost and not transferred to the columella.

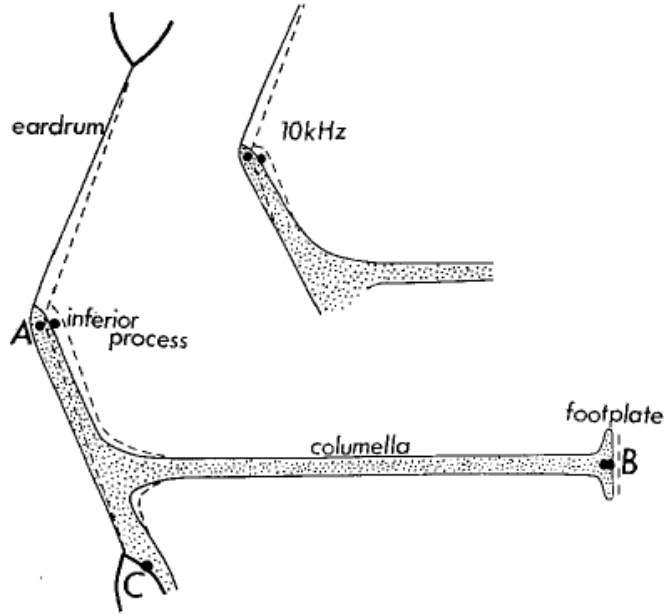


Figure 2.3: Operation of the middle ear lever in geckos reproduced from [14]. The inferior process of the extracolumella (A-C) hinges at point C at low frequencies. Also shown is the flection of the inferior process of the extracolumella.

Tympanic Membrane

The extracolumella applies a significant mechanical load on the tympanum and thereby precludes its treatment as a freely vibrating membrane. Furthermore, the contact surface of the malleus on the human eardrum is more or less symmetric whereas the extracolumella is attached asymmetrically. This has important physical consequences - especially in the observed vibration patterns of the membrane.

In the previous treatment of the ICE model, the tympanum was modelled as a clamped circular membrane with assymetrically attached sectoral load between $-\beta < \phi < \beta$ ([13]). This manifests itself as an additional boundary condition at $\phi = \beta$ and $\phi = -\beta$ which has to be satisfied via a numerical approximation. While this method has the advantage of being able to accurately reproduce the complex vibration patterns of the eardrum, it does not lend itself well to an analytical treatment of the coupled system.

In our study, we will follow a slightly different path. The tympanic membrane will be modelled as a rigidly clamped sectoral membrane. This means that in addition to the radial boundary at a_{tym} , we have a new set of boundaries at $\phi = \beta$ and $\phi = 2\pi - \beta$ where the membrane vibration is set to zero. This is illustrated in 2.4. The membrane material will be assumed to be linear-elastic. As before, the equations describing the vibrations of the membrane will consequently be linear 2nd-order PDE's.

At this point we should note that we have effectively set the mass of the extracolumella to infinity. Thereby, its motion has been neglected altogether. While this may seem counterintuitive at first, we will later see that this assumption, while simplifying the problem

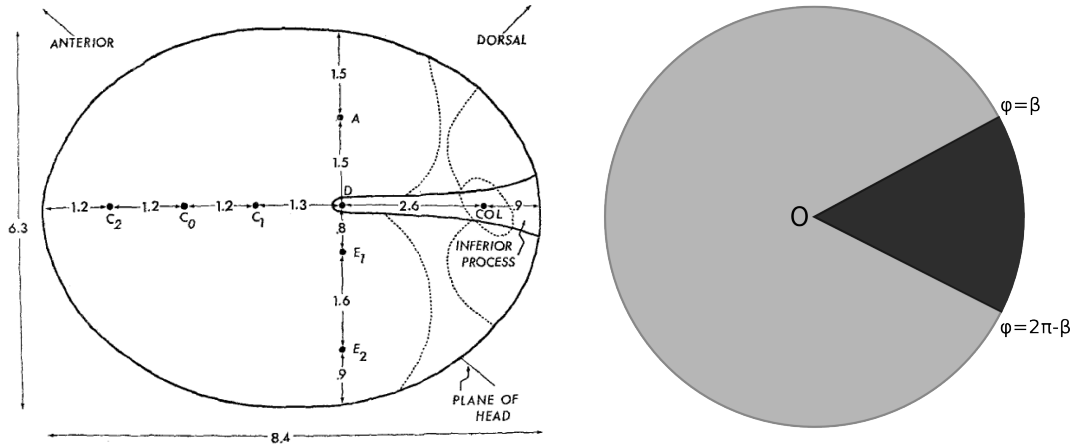


Figure 2.4: Left: Sketch of the eardrum of a Tokay gecko as seen from the outside taken from Manley, [15]. “COL” is the approximate position opposite the extracolumella insertion. The dots indicate the positions for measurements and will be discussed briefly in the next chapter. Dimensions in millimeters. Right: Our model for the loaded tympanic membrane. The lightly shaded region is modelled as a linear elastic membrane whereas the darkly shaded region ($\beta < \phi < 2\pi - \beta$) represents the contact surface of the extracolumella and the membrane. β corresponds to the breadth of the extracolumella and is estimated from anatomical data.

analytically, has little effect on the physical phenomenon of interest, viz. the coupling between the eardrums and the amplification of hearing cues. This will be discussed in-depth in Chapter 3.

2.1.3 Head Model and External Sound Input

In realistic environments the acoustic fields experienced by animals are often very complex. In addition to sound waves radiated directly from one or more sources in general, they also involve waves reflected from objects in their immediate neighbourhood. Higher animals such as humans possess the neural power to carry out the sophisticated signal processing needed to derive useful information from these signals. Simpler animals like geckos respond to simpler cues - usually the direct field from the nearest or strongest source.

We can therefore model our incoming wave as the simple case of an incident plane wave of a certain frequency. This input is specified in terms of its intensity, frequency and direction. Such a stimulus can be generated in an anechoic chamber from loudspeakers which are placed at a distance from the animal that is large compared to the animal’s size and the wavelength of the sound involved. Such experimental-setups are more thoroughly described by Christensen-Dalsgaard and Manley ([4], [16]) and Christensen-Dalsgaard, Tang and Carr ([17]).

The amplitude of the sound pressure incident on both ears can be taken as uniform in over the surface of the membrane. The spatial variation can be safely neglected because the typical eardrum is less than 5mm in diameter whereas the smallest sound wavelengths in

the hearing range of the larger lizards (eg. Tokay gecko) is around 70mm (4000 Hz) and is around 50mm (7000 Hz) for the smaller lizards (eg. Hemidactylus). In other experiments, a similar stimulus has also been provided by means of a headphone sealed to the ear ([18]).

In general the sound on the other side of the head will differ in phase as well as amplitude. This is a result of the diffraction of sound around the head and body of the animal. The exact variation depends on the size of the animal and the frequency of the incident wave. Due to the typically small head size of geckos, the amplitude variation (known as shadowing) is negligible ([7]). The phase difference, although small compared to those in larger animals, cannot be neglected. We can therefore consider the sound wave with angular frequency ω to have a constant (pressure) amplitude p on the head.

In the earlier ICE model, the effect of diffraction on the phase difference was neglected as well. The phase difference is found directly from the phase difference Δ as shown in fig. 2.5. As a result, the sound pressure inputs at both ears is given by,

$$p_0 = pe^{j\omega t} e^{j\Delta/2}, \quad p_L = pe^{j\omega t} e^{-j\Delta/2}, \quad \Delta = kL \sin \theta. \quad (2.2)$$

We note that in defining the input in this way, we've emphasized the symmetry of the system. The ear closer to the sound source is referred to as the *ipsilateral* ear the one further away from the source is referred to as the *contralateral* ear. The terms ipsi- and contralateral also refer to the stimuli meaning "the response of the ipsilateral ear" is equivalent to "the response of the ear to ipsilateral stimulus". We have also chosen a coordinate system relative to the *median-sagittal* plane or the head midline of the animal and θ gives the angle of incidence of this sound wave relative to this plane. For more complex auditory systems we would require two angles (θ, ϕ) to describe the three-dimensional system but in our analysis this is unnecessary. For the animals we are concerned with, i.e. geckos, the natural predators and prey are usually present on the same plane as the animal and our assumption is therefore reasonable. According our convention, $\theta = 0^\circ$ corresponds to objects directly in front of the animal and $\theta = \pm 180^\circ$ to objects directly behind. In our model we model the head as a sphere with a diameter equal to the interaural separation. As a result the sound has to travel around the head in order to reach the contralateral ear resulting in a longer path. The frequency domain solution for the diffraction of sound around a sphere was obtained by Lord Rayleigh at the end of the 19th century ([19],[20]). The expressions are greatly simplified at low frequencies and the phase difference is simply increased by by a factor of 1.5. The new model is illustrated in Fig. 2.6. Therefore, the form of the input remains the same as in (2.2) expect for a new phase difference $\Delta_{new} = 1.5\Delta$.

2.2 Derivation of the Model

We will now use the previously described physical model to derive the main expressions of interest in the ICE model - the membrane vibration profiles, the ipsi- and contraleteral filters and the cavity pressure distribution. We will thus find an expression for the pressure distribution in the cylindrical cavity and for the membrane vibrations subject to an external stimulus. After applying the appropriate boundary conditions to relate the membrane

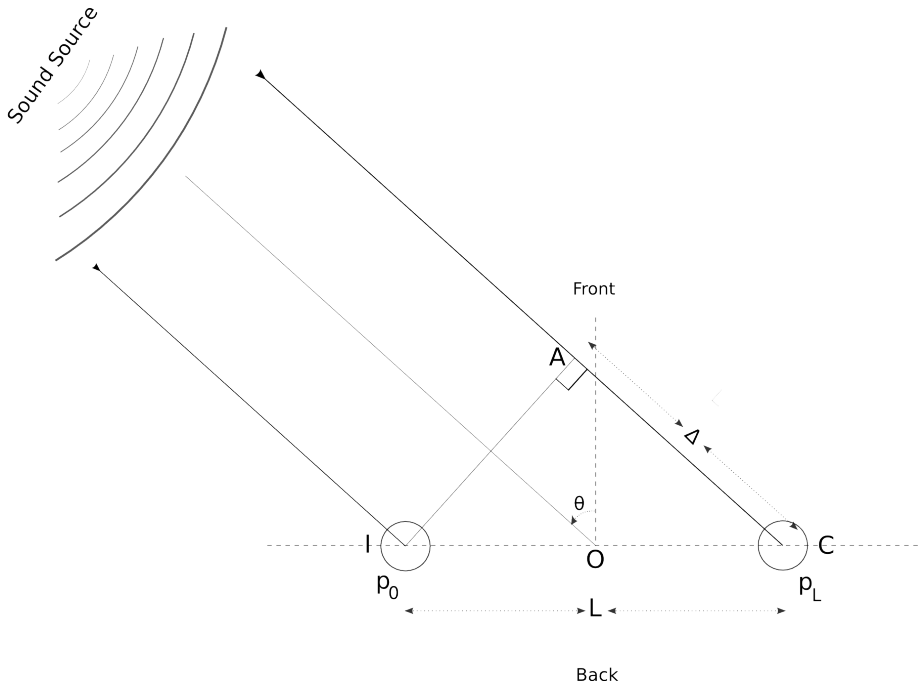


Figure 2.5: The previous acoustic head model for geckos. Depending on the angle of the sound source θ , the distance between the sound source and the contralateral ear is longer than its distance from the ipsilateral ear. The extra distance travelled by the sound wave to reach the contralateral ear is $L \sin \theta$ which gives rise to a phase difference $\Delta = kL \sin \theta$. However, this model neglects the increased phase difference due to diffraction effects which can be significant.

vibrations to the internal pressure, we will find the expression for the membrane vibrations as a function of direction and frequency.

We will start in Sec. 2.2.1 by finding a general solution to a 2nd-order PDE - the 3D wave equation - that describes the pressure distribution inside the cylindrical cavity. In this section we will introduce the main boundary condition the pressure will be subject to - the “no-penetration” boundary condition. This is a physical requirement that results from the fact that the air inside the cavity does not penetrate a solid boundary.

In Sec. 2.2.2 we will solve for the vibrations of the tympanic membranes. As an example, we will find an expression for the free and periodically driven vibrations of a circular membrane. Using the methods developed in this section, we will solve for the vibrations of a sectoral membrane - which, as we have already discussed, models the loaded tympanum. The final expression will correspond to the steady-state vibrations of a linear elastic membrane. As we neglect the transient response of the membrane, we will also discuss the circumstances under which this is justified.

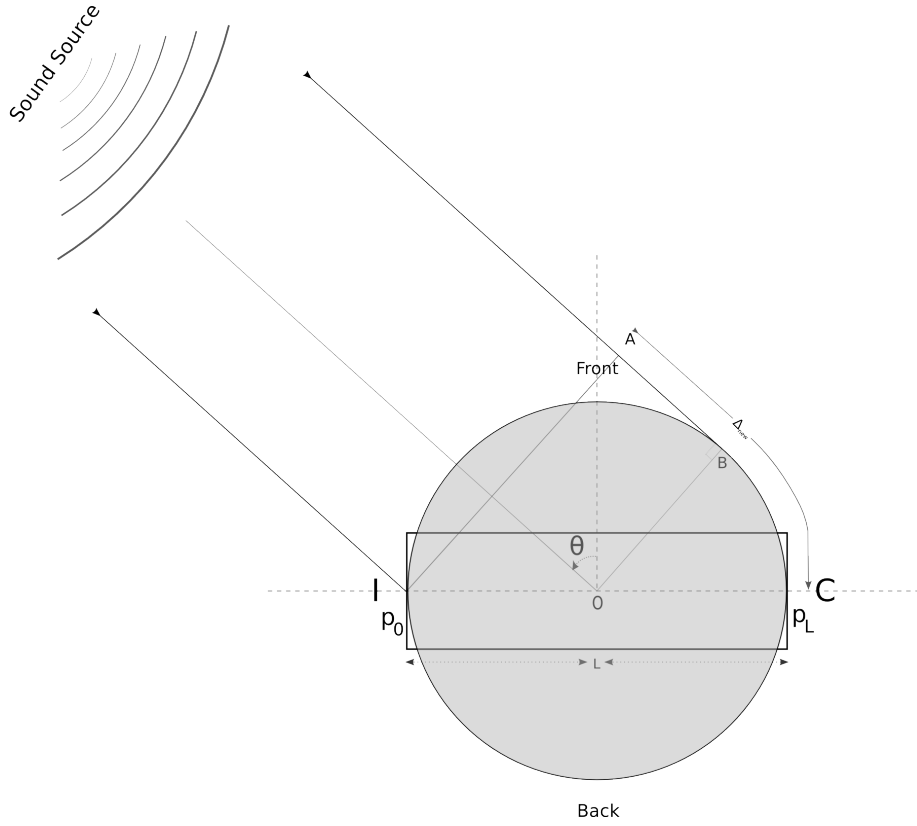


Figure 2.6: The acoustic head model for geckos. The rectangular outline is the internal cavity. As before, the sound wave has to travel an extra distance to reach the contralateral ear. In this case we have accounted for the influence of diffraction around the head on the phase difference between the inputs to both ears resulting in an increased phase difference $\Delta_{new} = 1.5\Delta$.

Table 2.1: Functions and Parameters used in the ICE Model

θ	Direction of the sound source with respect to the head midline.
ω	Angular frequency of the incoming sound wave.
k	Wavenumber $k = \omega/c$ with $c = 343\text{m/s}$ being the speed of sound.
p	Pressure amplitude of the incoming sound wave.
Δ	Phase difference between the sound wave reaching the contra- and ipsilateral ear.
$p_{0/L}$	Sound pressure on the ($x = 0$) and ($x = L$) tympani respectively.
(x, r, ϕ)	Cylindrical polar coordinates with x being the axial direction.
L	Interaural separation and length of cylinder.
a_{cyl}	Radius of cylinder.
a_{tym}	Radius of tympanum.
$\beta < \phi < 2\pi - \beta$	Extent of the vibrating part of the membrane. The rest of the circle corresponds to the extracolumellar footplate.
V_{cav}	Volume of the cavity.

In Sec. 2.2.3 we will conclude by using our knowledge to solve for the vibration of the fully coupled system. In this section we will proceed by applying the velocity boundary condition at either end of the cylinder. In order to help with our analysis, we will present a simplification scheme for this boundary condition. We will end this section by defining the ipsi- and contralateral filters. The final expressions that give us the vibrations of the tympanic membranes as a function of the external pressure with the influence of the internal cavity encoded in the ipsi- and contralateral filters. We have listed the main parameters and functions used in our analysis (including the geometry parameters) in Tables 2.1 and 2.2.

Table 2.2: Functions and Parameters used in the ICE Model contd.

J_q	Order q Bessel function of the first kind.
μ_{qs}, ν_{qs}	Respectively - s^{th} zero and s^{th} extremum of the above Bessel function.
$f_{qs}(x, r, \phi)$	Orthogonal modes for the pressure distribution inside the mouth cavity.
ζ_{qs}	Wavenumber of the above modes in the x -direction.
$p(x, r, \phi; t)$	Pressure distribution inside the mouth cavity.
$v_x(x, r, \phi; t)$	Velocity function inside the mouth cavity.
$u_{mn}(r, \phi; t)$	Eigenmodes of the membrane displacement function.
ω_{mn}	Eigenfrequency of the above eigenmodes.
Q	Quality factor of the membrane.
$\Psi(r, \phi; t)$	Driving pressure on the membrane.
$u_{0/L}(r, \phi; t)$	Membrane displacement function.
$C_{mn}^{0/L}$	Membrane vibration expansion coefficients.
$S^{0/L}(t)$	Total membrane displacement.
$G_{ipsi}(r, \phi)$	Ipsilateral filter.
$G_{contra}(r, \phi)$	Contralateral filter.

2.2.1 Internal Cavity

We assume that the air inside the cavity obeys linear acoustics (cf. acoustic textbooks such as [21, p. 313] and [22, p. 247]). This means that the air moves due to pressure $p(x, r, \phi; t)$ whose distribution inside the cavity is given by the 3D acoustic wave-equation in cylindrical polar coordinates,

$$\frac{1}{c^2} \frac{\partial^2 p(x, r, \phi, t)}{\partial t^2} = \frac{1}{r} \frac{\partial}{\partial r} \left(r \frac{\partial p(x, r, \phi, t)}{\partial r} \right) + \frac{1}{r^2} \frac{\partial p(x, r, \phi, t)}{\partial \phi^2} + \frac{\partial p(x, r, \phi, t)}{\partial x^2} \quad (2.3)$$

where c is the sound propagation velocity. The complete solution must take into account the boundary conditions at and within the cavity walls and the ones at the air-membrane interface. We also note that the above equation implies that the animal's mouth is closed,

which is typical for a waiting animal. In order to solve (2.3) for a particular frequency f (angular frequency $\omega = 2\pi f$), we use the following separation ansatz

$$p(x, r, \phi, t) = f(x)g(r)h(\phi)e^{j\omega t} \quad (2.4)$$

which after substitution into the acoustic wave-equation leads to,

$$\begin{aligned} k^2 f(x)g(r)h(\phi) + f(x)h(\phi) & \left[\frac{\partial^2 g(r)}{\partial r^2} + \frac{1}{r} \frac{\partial g(r)}{\partial r} \right] \\ & + f(x)g(r) \frac{1}{r^2} \frac{\partial h(\phi)}{\partial \phi} + \frac{\partial^2 f(x)}{\partial x^2} = 0 \end{aligned} \quad (2.5)$$

with $k := \omega/c$. This results in the following set of separated ODE's,

$$\frac{d^2 f(x)}{dx^2} + \zeta^2 f(x) = 0 \quad (2.6)$$

$$\frac{d^2 h(\phi)}{d\phi^2} + q^2 h(\phi) = 0 \quad (2.7)$$

$$\frac{\partial^2 g(r)}{\partial r^2} + \frac{1}{r} \frac{\partial g(r)}{\partial r} + \left[\underbrace{(k^2 - \zeta^2)}_{=: \nu^2} - \frac{q^2}{r^2} \right] g(r) = 0 \quad (2.8)$$

with separation constants q and ζ . The last equation is the Bessel differential equation [23, p. 313] and its general solution is given by,

$$g(r) = C_{qs} J_q(\nu r) + D_{qs} Y_q(\nu r). \quad (2.9)$$

J_q and Y_q are the order- q Bessel functions of the first and second kind respectively. The Bessel function of the second kind can be ignored as it diverges at $r = 0$. The solutions to the separated equations are therefore given by,

$$f(x) = e^{\pm \zeta x}, \quad h(\phi) = e^{\pm j\phi}, \quad \text{and} \quad g(r) = J_q(\nu r) \quad (2.10)$$

with a specific solution to (2.3) given by,

$$p(x, r, \phi; t) = [(A^+ e^{jq\phi} + A^- e^{-jq\phi})e^{j\zeta x} + (B^+ e^{jq\phi} + B^- e^{-jq\phi})e^{-j\zeta x}] J_q(\nu r) e^{j\omega t}. \quad (2.11)$$

The coefficients A^\pm , B^\pm , q , ζ and ν will be subsequently determined by the boundary conditions. Before we move on to the boundary conditions we should note that in general, the time component of the pressure also has a *backward-moving* component, i.e. $e^{-j\omega t}$. By making the ansatz in (2.4), we have implicitly made use of the fact that the form of the input as given in (2.2) constrains the pressure to only have a *forward-moving* component, i.e. $e^{j\omega t}$.

Pressure Boundary Conditions

There are three sets of boundary conditions -

- Continuity and smoothness in ϕ which is equivalent to $h(0) = h(2\pi)$ and $h'(0) = h'(2\pi)$ where, $h' = dh/d\phi$.
- Vanishing of the normal derivative at the cavity walls - $g'(a_C) = 0$ (a_C is the radius of the cylinder).
- Equating the membrane velocity to the velocity function at the membrane boundaries (to be discussed in the next section).

The first set of requirements is obvious. This reduces (2.11) to

$$p(x, r, \phi; t) = [Ae^{j\zeta x} + Be^{-j\zeta x}] \cos q\phi J_q(\nu r) e^{j\omega t}. \quad (2.12)$$

With q constrained to be an integer.

The second and third are a result of the so called “no-penetration” boundary-condition of fluid-mechanics. It arises from the fact that the cavity wall is an impermeable boundary. This translates into the requirement that the normal velocity function should vanish ([24, p. 111]). The velocity function (\mathbf{v}) is related to the pressure by,

$$-\rho \frac{\partial \mathbf{v}}{\partial t} = \nabla p \quad (2.13)$$

At the cylindrical cavity wall, the normal velocity is in the radial direction. Substituting the expression for pressure in (2.11) in the above equation leads to a Neumann boundary condition for the pressure,

$$\begin{aligned} v_r &= -\frac{1}{j\rho\omega} \frac{\partial p(x, r, \phi; t)}{\partial r} \Big|_{r=a_C} = 0 \\ &\Rightarrow \frac{\partial J_q(\nu r)}{\partial r} \Big|_{r=a_C} = 0 \end{aligned} \quad (2.14)$$

This constrains ν to a discrete set of values which correspond to the local minima and maxima of J_q . We can therefore index ν by q and $s = 0, 1, 2, 3, \dots$ with $\nu_{qs} = z_{qs}/a_C$: z_{qs} being the s^{th} extremum of the order- q Bessel function of the first kind. This results in a discrete set of modes that satisfy (2.3) which are given by,

$$p_{qs}(x, r, \phi; t) = [A_{qs}e^{j\zeta_{qs}x} + B_{qs}e^{-j\zeta_{qs}x}] f_{qs}(r, \phi) e^{j\omega t} \quad (2.15)$$

where we have added the subscripts q and s to ζ and denoted the (r, ϕ) part of (2.12) by $f_{qs}(r, \phi)$. Effectively, the modes are 3D waves propagating with wave numbers ζ_{qs} in the x -direction and ν_{qs} in the radial direction. The first of these modes (corresponding to $q = 0, s = 0$) is of particular importance. Since the first maximum of J_0 occurs at $r = 0$,

we have $\nu_{00} = 0$. This leads to the first mode being a plane-wave which is constant in r and ϕ and only varies in x .

A very useful property of the above modes is their orthogonality, i.e.

$$\int_{\Omega} dV p_{q_1 s_1} p_{q_2 s_2} = 0, \text{ if } q_1 \neq q_2 \text{ or } s_1 \neq s_2 \quad (2.16)$$

the integral is over the volume of the cylinder. This is a consequence of the fact that for different q 's the cosine parts of the modes are orthogonal whereas for a given q the Bessel parts are orthogonal for different s 's or expressed as an equation,

$$\int dS f_{q_1 s_1} f_{q_2 s_2} = 0, \text{ if } q_1 \neq q_2 \text{ or } s_1 \neq s_2 \quad (2.17)$$

where $dS = r dr d\phi$ and the integral being taken over the disk of radius a_C . We can therefore write the general solution to (2.3) as a linear combination of the orthogonal modes given in (2.15),

$$p(x, r, \phi; t) = \sum_{q=0}^{\infty} \sum_{s=0}^{\infty} (A_{qs} e^{j\zeta_{qs} x} + B_{qs} e^{-j\zeta_{qs} x}) f_{qs}(r, \phi) e^{j\omega t} \quad (2.18)$$

The remaining coefficients, A_{qs} and B_{qs} , will be determined by equating the velocity function to the membrane velocity at both ends of the cylinder. To do so, we will first need to find an expression for the membrane vibrations - as we will in the following section.

2.2.2 Vibration of the Membrane

As a preliminary exercise, we will first derive expressions for the free and force-driven vibrations of a circular membrane. We will then use our results to move on to the sectoral membrane which corresponds to the tympanum loaded by the extracolumella. This corresponds to the approximating the extracolumella to have infinite mass.

Circular Membrane

The equation of motion for the vibration of a rigidly clamped circular membrane of radius a_M solves for the membrane displacement u at a point (r, ϕ) with $r < a$ and $0 < \phi < 2\pi$. It is given by,

$$\begin{aligned} -\frac{\partial^2 u(r, \phi; t)}{\partial t^2} - 2\alpha \frac{\partial u(r, \phi; t)}{\partial t} + c_M^2 \left[\frac{1}{r} \frac{\partial}{\partial r} \left(r \frac{\partial u(r, \phi, t)}{\partial r} \right) + \frac{1}{r^2} \frac{\partial^2 u(r, \phi, t)}{\partial \phi^2} \right] \\ = \frac{1}{\rho_M d} \Psi(r, \phi; t) \end{aligned} \quad (2.19)$$

subject to the boundary condition $u(r, \phi; t)|_{r=a_M} = 0$. We've defined the following membrane material properties,

- c_M - propagation speed of vibrations.

- $\alpha(> 0)$ - the damping coefficient.
- ρ_M - density.
- d - thickness.

$\Psi(r, \phi; t)$ is the pressure on the membrane surface at (r, ϕ) . In our discussion we are only concerned with periodic and uniform pressure acting on the membrane surface. As we have already stated in Sec. 2.1.3, the small size of the membrane with respect to the sound wavelength, justifies the spatial uniformity of our input.

Free Vibrations

Undamped Membrane: We first determine the eigenmodes of an undamped circular membrane by solving (2.19) for $\alpha = 0$, $\Psi = 0$ (the resultant equation is better known as the 2D Helmholtz equation, cf. [25, p. 187]). Just as we did in (2.4), we do this by making a separation ansatz ,

$$u(r, \phi; t) = f(r)g(\phi)h(t) \quad (2.20)$$

This gives us the following set of equations

$$\frac{\partial^2 f(r)}{\partial r^2} + \frac{1}{r} \frac{\partial f(r)}{\partial r} + \left[\mu^2 - \frac{m^2}{r^2} \right] f(r) = 0 \quad (2.21)$$

$$\frac{d^2 g(\phi)}{d\phi^2} + m^2 g(\phi) = 0 \quad (2.22)$$

$$\frac{d^2 h(t)}{dt^2} + c_M^2 \mu^2 h(t) = 0 \quad (2.23)$$

with separation constants μ and m . The solution of the first of these equations should already be familiar to us from the previous section - $J_m(\mu r)$, the order- m Bessel function of the first kind. The boundary conditions in ϕ direction remain the same resulting in,

$$u(r, \phi; t) = [(M^+ e^{jm\phi} + M^- e^{-jm\phi}) e^{jc_M \mu t} + (N^+ e^{jm\phi} + N^- e^{-jm\phi}) e^{-jc_M \mu t}] J_m(\mu r) \quad (2.24)$$

Unlike in the case of the internal cavity, we require u to vanish at the boundary so we have a Dirichlet boundary condition which effectively requires: $J_m(\mu a_M) = 0$. This constrains μ to a discrete set of values which correspond to the zeros of J_m . The eigenmodes of a the circular membrane are therefore given by,

$$u_{mn}(r, \phi; t) = [(M_{mn}^+ e^{jm\phi} + M_{mn}^- e^{-jm\phi}) e^{j\omega_{mn} t} + (N_{mn}^+ e^{jm\phi} + N_{mn}^- e^{-jm\phi}) e^{-j\omega_{mn} t}] J_m(\mu_{mn} r) \quad (2.25)$$

where $\mu_{mn} = z_{mn}/a_M$, z_{mn} being the n^{th} zero of J_m and, $\omega_{mn} = c_M \mu_{mn}$ is the eigenfrequency of the (m, n) eigenmode. At this point m can take any positive real value – a fact that will help us solve the sectoral membrane problem. However, in the case of a full circular

membrane – as in the case of the pressure inside a cylindrical cavity – requirements of continuity and smoothness in ϕ reduce (2.25) to,

$$u_{mn}(r, \phi; t) = \cos m\phi J_m(\mu_{mn}r) [M_{mn}e^{j\omega_{mn}t} + N_{mn}e^{-j\omega_{mn}t}] \quad (2.26)$$

with $m = 0, 1, 2, \dots$ with the (m, n) eigenmodes forming an orthogonal set. For later convenience we denote the spatial part of the above mode by $u_{mn}(r, \phi)$. The first few of these modes are plotted in 2.7.

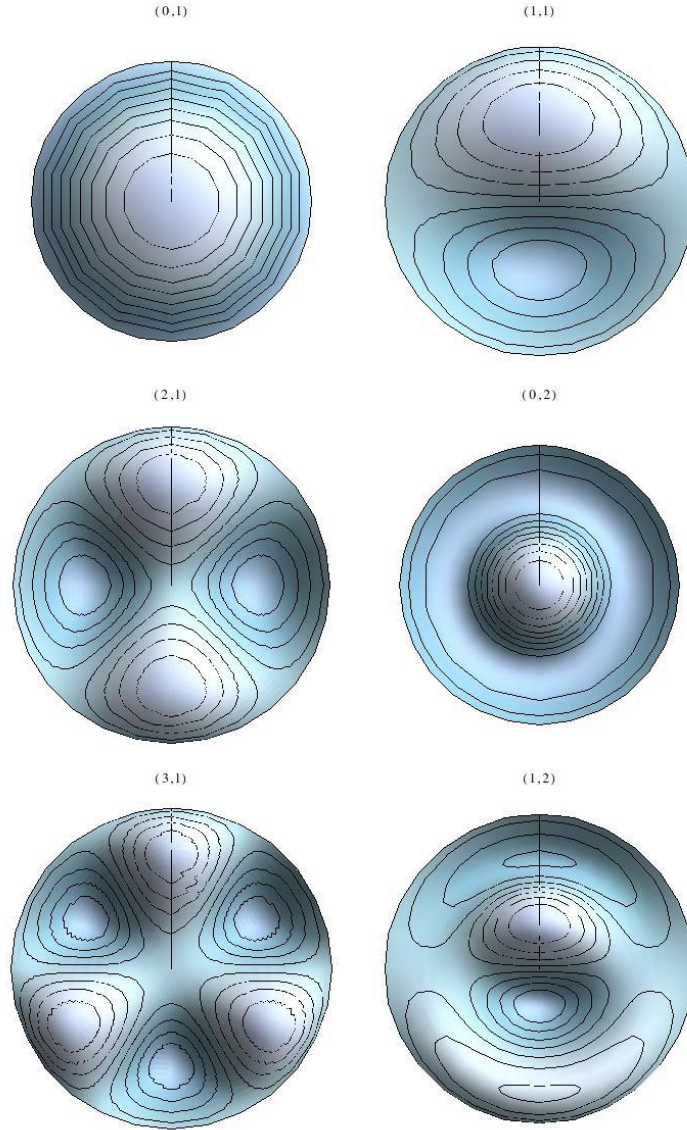


Figure 2.7: Eigenmodes of a full circular membrane. The eigenfrequency increases from left to right.

We note that unlike in the case of the internal cavity, the free membrane has components that are both forward- and backward-moving in time. The presence of a driving force,

however, will result in simpler expressions. This will be discussed in more detail in the next chapter where we compare our model with experimental data.

Damped Membrane: For a damped membrane, i.e. $\alpha \neq 0$, the spatial part of the above eigenmodes remains the same. The form of the time-dependent part is given by the solution of the equation,

$$\frac{d^2 h_{mn}(t)}{dt^2} + 2\alpha \frac{dh_{mn}(t)}{dt} + \omega_{mn}^2 h_{mn}(t) = 0. \quad (2.27)$$

Assuming h_{mn} takes the form $e^{j\tilde{\omega}_{mn}}$ leads to a quadratic equation with solutions,

$$\tilde{\omega}_{mn} = j\alpha \pm \omega_{mn}^* \quad (2.28)$$

$$\omega_{mn}^* = \sqrt{\alpha^2 + \omega_{mn}^2} \quad (2.29)$$

We require the membrane displacement to remain finite as $t \rightarrow \infty$. We can therefore neglect the $e^{-j\tilde{\omega}_{mn}}$ terms leading to,

$$\tilde{u}_{mn}(r, \phi; t) = \cos m\phi J_m(\mu_{mn}r) [M_{mn} e^{j\omega_{mn}^* t} + N_{mn} e^{-j\omega_{mn}^* t}] e^{-\alpha t} \quad (2.30)$$

The general solution is given by a linear combination of the above and the coefficients are determined by initial conditions – for example, membrane displacement and velocity at $t = 0$.

Forced Vibrations

For a periodically driven membrane, there are two components of the full solution for forced vibrations. The first of these is the steady state solution which oscillates with the same frequency as the input and does not depend on the initial conditions - u_{ss} . The second of these is the transient solution that depends on the initial conditions but not on the driving pressure - u_t .

Steady State Solution: The steady state solution is expressed as a linear combination of the spatial part of the above eigenmodes and is given by,

$$u_{ss}(r, \phi; t) = \sum_{m=0}^{\infty} \sum_{n=1}^{\infty} C_{mn} \cos m\phi J_m(\mu_{mn}r) e^{j\omega t}. \quad (2.31)$$

Substituting this expression in (2.19) with $\Psi = pe^{j\omega t}$ gives,

$$\sum_{m=0}^{\infty} \sum_{n=1}^{\infty} \Omega_{mn} C_{mn} \cos m\phi J_m(\mu_{mn}r) e^{j\omega t} = pe^{j\omega t} \quad (2.32)$$

$$\text{where, } \Omega_{mn} = \rho_M d [(\omega^2 - \omega_{mn}^2) - 2j\alpha\omega]. \quad (2.33)$$

Using the orthogonality of the eigenmodes, the coefficients C_{mn} can be calculated,

$$C_{mn} = \frac{p \int dS u_{mn}}{\Omega_{mn} \int dS u_{mn}^2} \quad (2.34)$$

with the integral this time being taken over the circular disk of radius a_M .

Transient Solution: The transient solution is effectively a solution of the free damped membrane, i.e. a linear combination of the eigenmodes given in (2.30). Therefore,

$$u_t(r, \phi; t) = \sum_{m=0}^{\infty} \sum_{n=1}^{\infty} \cos m\phi J_m(\mu_{mn}r) [M_{mn}e^{j\omega_{mn}^* t} + N_{mn}e^{-j\omega_{mn}^* t}] e^{-\alpha t}. \quad (2.35)$$

The complete solution is given by $u = u_t + u_{ss}$ and the coefficients M_{mn} and N_{mn} are determined by the initial conditions (at $t = 0$).

Steady State Approximation: The damping coefficient α is usually given in terms of the membrane fundamental frequency and a quality factor Q as $\alpha = \omega_{01}/2Q$. The tympani we will be concerned with are generally underdamped to critically damped i.e. $Q \geq .5$ which results in damping coefficients that are around $2400s^{-1}$ for the larger lizards and around $7700s^{-1}$ for the smaller ones (the exact parameter values will be discussed in the next chapter). Due to this and the exponential decay of the transient vibration amplitude, we can safely assume that within a few time-periods the transient vibrations forced membrane will be negligible. For this reason, we will subsequently confine our discussion to only the steady state vibrations of the membrane.

Sectoral Membrane

The eigenmodes of the sectoral membrane proceeds from (2.25) onwards. We now have a new set of boundary conditions in ϕ . The extracolumella is modelled as a triangular plate of infinite mass which constrains the membrane displacement to go to zero at $\phi = \beta$ and $\phi = 2\pi - \beta$. This results in the following set of eigenmodes,

$$u_{mn}(r, \phi; t) = \sin \kappa(\phi - \beta) J_\kappa(\mu_{mn}r) [M_{mn}e^{j\omega_{mn}t} + N_{mn}e^{-j\omega_{mn}t}] \quad (2.36)$$

where $\kappa[m] = \frac{m\pi}{2(\pi - \beta)}$, $m = 1, 2, 3, \dots$. We see that the r part of the above mode is given by the order- κ Bessel function of the first kind; μ_{mn} being its n^{th} zero, as before. The solution for the damped membrane follows in an identical way. It is apparent from the form of the above modes that, unlike in the case of the circular membrane eigenmodes, these modes are no longer circularly symmetric. We plot the first few of these modes in 2.8. The solution for forced membrane vibrations follows in the same way as in the circular membrane case. The vibrations of a sectoral membrane are discussed in more detail in [26, p. 87]. As discussed earlier, the sectoral shape of the membrane has important physical consequences and captures the complex vibration patterns of a realistic membrane. This will be discussed in the next chapter.

2.2.3 Vibration of Coupled Membranes

With our current knowledge, we can move on to the main part of the chapter - the vibration of coupled membranes. It is convenient to first write down the main equations of the system

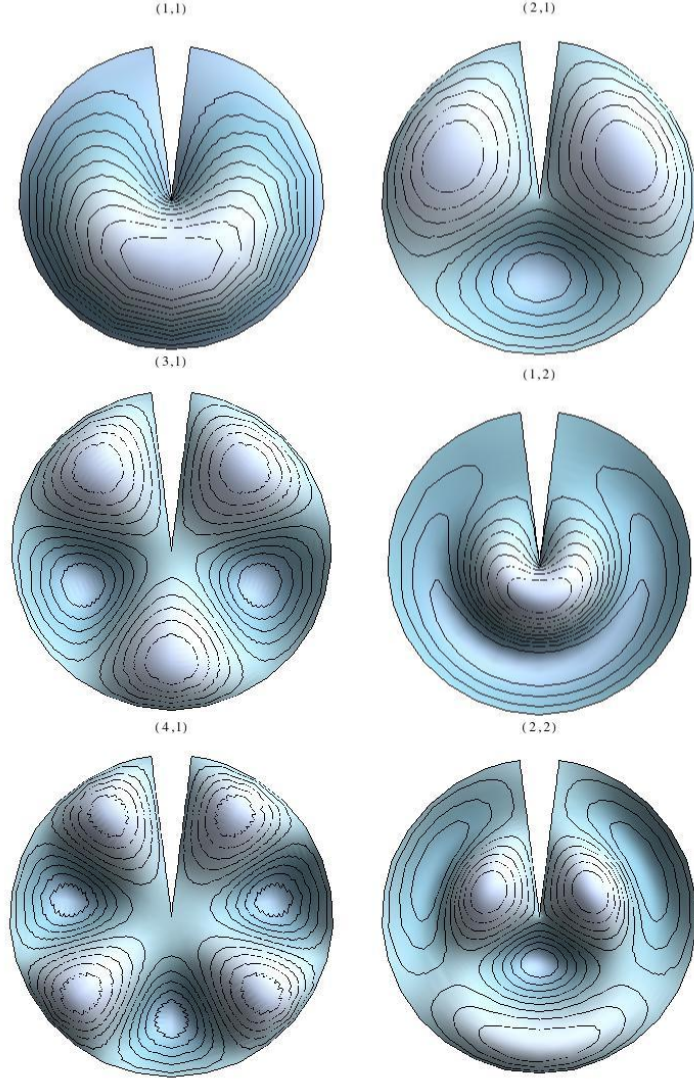


Figure 2.8: Eigenmodes of a sectoral membrane where the omitted region corresponds to the extracolumnella with $\beta = \pi/25$. As in Fig. 2.7, the eigenfrequency increases from left to right.

based on our previously derived expressions. The vibrations of the membranes is given by,

$$u_{0/L}(r, \phi; t) = \sum_{m=0}^{\infty} \sum_{n=1}^{\infty} \Omega_{mn} C_{mn}^{0/L} u_{mn}(r, \phi) e^{j\omega t} = p_{0/L} e^{j\omega t} - p(0/L, r, \phi; t) \quad (2.37)$$

where 0 and L denote the $x = 0$ and $x = L$ membranes respectively and the cavity pressure distribution, $p(x, r, \phi; t)$, is given by (2.18). The above equation is only valid on the membrane surface i.e., for $r < a_{typ}$ and $\beta < \phi < 2\pi - \beta$.

As discussed in 2.2.1, the internal cavity pressure satisfies the no-penetration condition at solid boundaries. This means that at both ends of the cylinder, we equate the velocity profile of air to the velocity profile of the circular surface including the membrane. This is

because the membrane diameter is smaller than the cylinder diameter. As a result, we will have to set the air-particle velocity to zero for $r > a_{tym}$. Since the membrane displacement is only in the x -direction, we only need to calculate the same component of the velocity. Using the relation (2.13) we get,

$$v_x(x, r, \phi; t) = -\frac{1}{\rho\omega} \sum_{q=0}^{\infty} \sum_{s=0}^{\infty} \zeta_{qs} (A_{qs} e^{j\zeta_{qs}x} - B_{qs} e^{-j\zeta_{qs}x}) f_{qs}(r, \phi) e^{j\omega t} \quad (2.38)$$

and the exact boundary conditions are given by,

$$j\omega U_0 = -v_x(0, r, \phi; t) \quad (2.39)$$

$$j\omega U_L = v_x(L, r, \phi; t) \quad (2.40)$$

where we've used the direction conventions described in 2.1 and made the following definition,

$$U_{0/L} = \begin{cases} u_{0/L}, & 0 < r < a_{tym} \text{ and } \beta < \phi < 2\pi - \beta \\ 0, & \text{otherwise} \end{cases} . \quad (2.41)$$

This in order to ensure that the boundary condition is satisfied over either end of the cylinder and not just over the membrane surface.

Approximate Boundary Condition

As previously stated, the exact boundary condition would entail setting the velocity function to be exactly equal to the membrane displacement velocity. At this point, it is important to note that the internal cavity eigenmodes are **not** orthogonal to the membrane eigenmodes in general². This means that every membrane eigenmode couples with every cavity eigenmode and that each of the coefficients A_{qs} and B_{qs} will be given by an infinite linear combination of the coefficients $C_{mn}^{0/L}$.

The first step in overcoming this problem is to rewrite the left-hand sides of the boundary conditions given in (2.39) and (2.40). We first expand U_0 and U_L in the orthogonal basis of the functions f_{qs} ,

$$U_{0/L}(r, \phi; t) = \sum_{q=0}^{\infty} \sum_{s=0}^{\infty} S_{qs}^{0/L} f_{qs}(r, \phi) e^{j\omega t} \quad (2.42)$$

$$\text{where, } S_{qs}^{0/L} = \frac{\int dS U^{0/L} f_{qs}(r, \phi)}{\int dS f_{qs}^2(r, \phi)} \quad (2.43)$$

We now have an expansion that approximates the boundary condition with increasing accuracy. After choosing an appropriate cutoff for the expansion we can substitute this expression in place of $U_{0/L}$ in (2.39) and (2.40). In fact, this cutoff in the boundary

²This would also be true if we had full circular membranes on either end of the cylinder. In this case we would have the added simplification that only the circularly symmetric cavity eigenmodes will be activated.

condition expansion results in an identical cutoff in the pressure expansion - a direct result of the orthogonality of the pressure modes.

We will now illustrate a solution to the problem by solving the problem with the zeroeth order boundary conditions. In the end, it will turn out that for our purposes the zeroeth order, i.e. the $(0, 0)$ mode is sufficient as higher modes only have a significant contribution at frequencies well above the hearing range of geckos. For example, the wavenumber of the $(1, 1)$ mode is above 33kHz for the cylindrical cavity corresponding to the house gecko and above 15kHz for the one corresponding to the Tokay gecko. The parameters used to derive these quantities will be discussed in the next chapter. We can therefore write the approximate boundary conditions to zeroeth order as,

$$\rho\omega^2 S^0 = - \sum_{q=0}^{\infty} \sum_{s=0}^{\infty} j\zeta_{qs} (A_{qs} - B_{qs}) f_{qs}(r, \phi) \quad (2.44)$$

$$\rho\omega^2 S^L = \sum_{q=0}^{\infty} \sum_{s=0}^{\infty} j\zeta_{qs} (A_{qs} e^{j\zeta_{qs} L} - B_{qs} e^{-j\zeta_{qs} L}) f_{qs}(r, \phi) \quad (2.45)$$

As shown in Sec. 2.2.1, the $(0, 0)$ mode only varies in the x -direciton. As a result, the left-hand sides of the above equation are nothing but the average displacement of the membrane surface given by,

$$S^{0/L} = \frac{\int dS U^{0/L}(r, \phi)}{\pi a_{cyl}^2}. \quad (2.46)$$

We have also omitted the “ qs ” subscript from $S^{0/L}$. Given the external parameters and boundary conditions, it only depends on time. We have effectively approximated the surfaces at 0 and L (including the membranes) by pistons moving with the average velocity of the total surface.

Given these boundary conditions, it is straightforward to calculate the coefficients A_{qs} and B_{qs} in terms of $S_{0/L}$. To do this we need to make use of the orthogonality relation given in (2.17). We do this by multiplying both sides of (2.44) and (2.45) by $f_{qs}(r, \phi)$ and integrate over the circular surfaces at either end of the cylinder. This results in a system of two linear equations for each pair of A_{qs} and B_{qs} ,

$$A_{qs} - B_{qs} = -L_{qs} \rho \omega^2 S^0 \quad (2.47)$$

$$A_{qs} e^{j\zeta_{qs} L} - B_{qs} e^{-j\zeta_{qs} L} = L_{qs} \rho \omega^2 S^L \quad (2.48)$$

$$\text{where, } L_{qs} = \frac{\int dS f_{qs}(r, \phi)}{j\zeta_{qs} \int dS f_{qs}^2(r, \phi)}$$

We now make use of the property of the pressure modes that $f_{qs}(r, \phi)$ integrates to 0 unless $q = 0$ and $s = 0$. For $q = 0$ this is a consequence of the Bessel functions integrating to zero while for $q \geq 1$ this is due to the more obvious fact that the integral of the cosine function from 0 to 2π is zero. As a result we have $A_{qs} = B_{qs} = 0$ for all modes except the $(0, 0)$ mode. In other words, the zeroeth-order boundary condition only supports

plane wave modes inside the cavity. We will subsequently omit the subscripts “00” for these coefficients. From the above linear equations, they are given in terms of the total membrane displacement as,

$$A = -\frac{\rho\omega^2}{2k \sin kL} (S^0 e^{-jkL} + S^L), \quad B = -\frac{\rho\omega^2}{2k \sin kL} (S^0 e^{jkL} + S^L) \quad (2.49)$$

we have also directly substituted $\zeta_{00} = k$ and simplified the expression for K_{00} in the above expressions. These coefficients can now be substituted in place of the pressure in the right-hand side of the equation (2.37) giving us,

$$\sum_{m=0}^{\infty} \sum_{n=1}^{\infty} \Omega_{mn} C_{mn}^0 u_{mn}(r, \phi) = p_0 + \frac{\rho\omega^2}{k} (S^0 \cot kL + S^L \csc kL) \quad (2.50)$$

$$\sum_{m=0}^{\infty} \sum_{n=1}^{\infty} \Omega_{mn} C_{mn}^L u_{mn}(r, \phi) = p_L + \frac{\rho\omega^2}{k} (S^0 \csc kL + S^L \cot kL) \quad (2.51)$$

where we have cancelled out the time component on both sides of the equations. Note that the right-hand sides of the above two equations are independent of the spatial (r, ϕ) coordinates.

In order to simplify the above coupled system of equations, the next step will be to take their sum and difference to obtain a new set of variables that are solutions of a pair of decoupled equations. After some algebraic manipulation, we therefore have

$$\sum_{m=0}^{\infty} \sum_{n=1}^{\infty} \Omega_{mn} C_{mn}^+ u_{mn}(r, \phi) = p_+ + \frac{\rho\omega^2}{k} S^+ \cot \frac{kL}{2} \quad (2.52)$$

$$\sum_{m=0}^{\infty} \sum_{n=1}^{\infty} \Omega_{mn} C_{mn}^- u_{mn}(r, \phi) = p_- - \frac{\rho\omega^2}{k} S^- \tan \frac{kL}{2} \quad (2.53)$$

where, $C_{mn}^+ = C_{mn}^L + C_{mn}^0$ and $C_{mn}^- = C_{mn}^L - C_{mn}^0$. The $S^{+/-}$ and $p_{+/-}$ terms are defined similarly. Now, analogous to the calculation of the coefficients for the steady state vibration in (2.32) and (2.34), we can determine the coefficients of the sum and difference vibrations in terms of the pressure and total membrane displacements. This gives us,

$$C_{mn}^+ = \left[p_+ + \frac{\rho\omega^2}{k} S^+ \cot \frac{kL}{2} \right] K_{mn} \quad (2.54)$$

$$C_{mn}^- = \left[p_- - \frac{\rho\omega^2}{k} S^- \tan \frac{kL}{2} \right] K_{mn} \quad (2.55)$$

$$\text{where, } K_{mn} = \frac{\int dS u_{mn}}{\Omega_{mn} \int dS u_{mn}^2}$$

The next step will be to multiply both sides of (2.54) and (2.55) with the integral $\int dS u_{mn}$, divide by πa_{cyl}^2 (the integral of f_{00}^2 as it appears in the denominator in (2.43)) and sum

over m and n . It is clear that the left hand sides become equal to $S^{+/-}$; this allows us to give exact expressions for the total membrane displacements.

$$S^+ = \frac{p_L + p_0}{\Lambda + \Gamma_+} \quad S^- = \frac{p_L - p_0}{\Lambda + \Gamma_-} \quad (2.56)$$

where we've defined the following quantities,

$$\Gamma_+ = -\frac{\rho\omega^2}{k} \cot \frac{kL}{2}, \quad \Gamma_- = \frac{\rho\omega^2}{k} \tan \frac{kL}{2} \quad (2.57)$$

$$\frac{1}{\Lambda} = \frac{1}{\pi a_{cyl}^2} \sum_{m=0}^{\infty} \sum_{n=1}^{\infty} \frac{(\int dS u_{mn})^2}{\Omega_{mn} \int dS u_{mn}^2} \quad (2.58)$$

We can finally write the membrane displacement as a function of the pressure inputs in the form

$$u_0(r, \phi; t) = G_{ipsi}(r, \phi)p_0 + G_{contra}(r, \phi)p_L \quad (2.59)$$

$$u_L(r, \phi; t) = G_{contra}(r, \phi)p_0 + G_{ipsi}(r, \phi)p_L \quad (2.60)$$

with the ipsilateral filter,

$$G_{ipsi} = \left(\frac{1}{\Lambda + \Gamma_+} + \frac{1}{\Lambda + \Gamma_-} \right) \sum_{n=1}^{\infty} \frac{\Lambda K_{mn}}{2} u_{mn}(r, \phi; t) \quad (2.61)$$

and the contralateral filter,

$$G_{contra} = \left(\frac{1}{\Lambda + \Gamma_+} - \frac{1}{\Lambda + \Gamma_-} \right) \sum_{n=1}^{\infty} \frac{\Lambda K_{mn}}{2} u_{mn}(r, \phi; t) \quad (2.62)$$

The total membrane displacement can also be expressed as a function of p_0 and p_L simply by integrating both sides of (2.59) and (2.60) giving us a new set of ipsi- and contralateral filters

$$G_{ipsi}^s = \left(\frac{1}{\Lambda + \Gamma_+} + \frac{1}{\Lambda + \Gamma_-} \right) / 2 \quad (2.63)$$

$$G_{contra}^s = \left(\frac{1}{\Lambda + \Gamma_+} - \frac{1}{\Lambda + \Gamma_-} \right) / 2 \quad (2.64)$$

The ipsilateral filter effectively gives us the response of the membrane to a purely ipsilateral stimulus or equivalently when the contralateral membrane is blocked. Similarly, the contralateral filter gives us its response when the ipsilateral membrane is blocked. These filters will play an important role in the evaluation of the model in the next chapter. Before we move on it is important to note that since Λ is an infinite series, in numerical analyses it has to be approximated by choosing an appropriate membrane mode cutoff. The choice of this cutoff depends on parameters specific to the animal; cf. Sec. 3.1.3. The basic method involves arranging the modes in increasing order of eigenfrequency (or equivalently μ_{mn}). As a result, we can express the summation over a single index. In general, for the frequency ranges of the animals we are concerned with, we will not need to calculate the summation beyond the first 20 eigenmodes.

2.2.4 Circuit Model

Before we conclude this chapter, we will discuss the previous methods used to model ears coupled through an air cavity. This method was used by Christensen-Dalsgaard and Manley in [4] and [16] and was based on methods presented in [26]. The method treats the problem through the analogy of electrical circuits and deals with low-frequency and high-frequency regimes separately.

In these models, the sound inputs are treated as voltage sources and the system is broken down into components, e.g. membranes, cavities, apertures which are modelled as lumped elements. Their impedance values depend on the geometry and material properties and in general can be resistive and reactive. The “current” is given by something called the “acoustic flow” which has the dimensions of volume per unit time. In the previous analysis, this is given by $j\omega\pi a_{cyl}^2 S^{0/L}$.

The low frequency circuit analog for the ICE model is illustrated in Fig. 2.9. The impedances are calculated using the following formulae,

$$R_T = \frac{\omega_T L_T}{Q}, \quad L_T = \frac{\rho_M d}{\pi a_{tym}^2}, \quad C_T = \frac{1}{\omega_T^2 L_T} \quad (2.65)$$

$$R_V = 0, \quad L_V = 0, \quad C_V = \frac{V_{cav}}{\rho c^2} \quad (2.66)$$

where R , L and C are the resistance, impedance and capacitance of the quantities respectively with the total impedance given by $Z = R + j\omega L + 1/j\omega C$. ω_T is the first eigenfrequency of the membrane. It should immediately be apparent that the cavity impedance

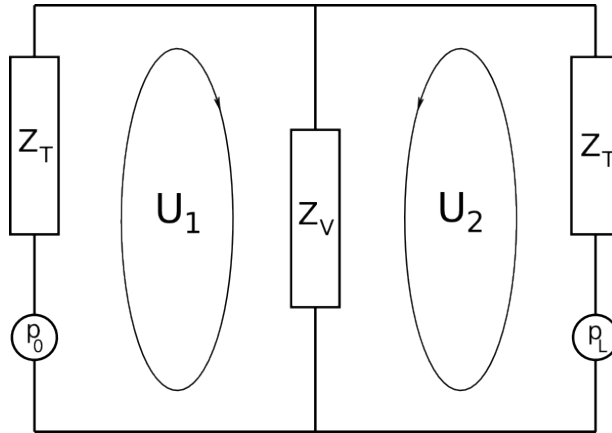


Figure 2.9: Low frequency circuit analog for the ICE Model. The membrane impedances are denoted by Z_T and the impedance of the internal cavity is denoted by Z_V . The acoustic flows are given by U_1 and U_2 .

only depends on its volume. This is a result of the assumption that the air inside the cavity behaves like an adiabatic gas. The adiabatic equation of state can then be used to determine the instantaneous pressure from the instantaneous volume change due to the

membrane motion which, after linearization, results in a uniform pressure inside the cavity. In addition, the membrane impedance Z_T only includes the effect of the first eigenmode. Also, Z_T includes the effect of the transducer which, in our case, is the extracolumella. Upon solving the circuit equations, the acoustic flows are calculated to be,

$$U_1 = \frac{p_0(Z_T + Z_V) - p_L Z_V}{Z_T(Z_T + 2Z_V)}, \quad U_2 = \frac{p_L(Z_T + Z_V) - p_0 Z_V}{Z_T(Z_T + 2Z_V)}. \quad (2.67)$$

At first glance the above results look very similar to total membrane displacements shown in (2.59) and (2.60). In fact, we can find the equivalent impedances from our analysis by comparing U_0 and U_L with the above results,

$$Z_T^{eq} = \frac{1}{j\omega\pi a_{cyl}^2}(\Lambda + \Gamma_-), \quad Z_V^{eq} = \frac{1}{2j\omega\pi a_{cyl}^2}(\Gamma_+ - \Gamma_-) \quad (2.68)$$

We immediately see that in the equivalent membrane impedance there is a correction term, Γ_- , which is a result of the contribution of the cavity whereas in the circuit model, the membrane impedance is determined independent of the cavity. Moreover, the equivalent standalone membrane impedance, Λ , includes the influence of the higher modes. The equivalent cavity impedance becomes equal to Z_V at zero frequency and goes to infinity at the resonance frequencies of the cylinder, i.e at $\omega = n\pi c/L$, $n = 1, 2, \dots$

We conclude this chapter by briefly stating the advantages of our method in comparison to the lumped element method -

- In terms of the membrane motion - we are able to account for the effect of asymmetrically loaded extracolumella and are able to describe the membrane motion in spatial detail.
- At low frequencies our model is consistent with the uniform pressure assumption but the nonuniformity steadily increases with frequency. We therefore have a single model that can describe both high- and low-frequency behaviour instead of treating the two regimes separately.

Chapter 3

Evaluation of the Model

We now have a complete geometrical representation of the ICE model as well as the analytical expressions u_0 and u_L that describe the membrane displacements in spatial detail as a function of direction and frequency. In this chapter we will use these variables to further study the features and predictions of our model and compare them with experimental results. In order to completely explain the observations, we will also need to estimate certain physical parameters like membrane eigenfrequency and quality factor that are important to our analysis but haven't yet been experimentally measured.

The main body of this chapter proceeds in Sec. 3.1 directly from the definitions given in (2.59) and (2.60). We will begin by assigning numerical values to the model parameters that have been defined in the previous chapter and comparing the membrane velocities of our model with experimentally determined values. We will then go on to define and study the two main quantities that serve as important localization cues - the Internal Time Differences (iTDS) and the Internal Level Differences (iLDs). These values model the possible neural subtractions that take place in the animal's brain in order to enhance directional sensitivity. Upon obtaining the spectral behaviour of these quantities, we will also be able to make an educated guess about the respective frequency ranges in which these cues are dominant and the possible range in which they could simultaneously be used. We will end this section by discussing possible methods to estimate parameter values that are difficult to measure. Finally, in Sec 3.2 we will compare the experimentally determined vibration pattern of the Tokay gecko's eardrum with that of our model's eardrum - the aim being to justify our choice for the geometry of the membrane.

In order to underline the fact that our model is universal model for internally coupled ears and not specialized to single species, we will compare our results for two gecko species - *Hemidactylus frenatus* or the common house gecko and the Tokay gecko. At the end of the chapter we will have an understanding of the advantages of a coupled system of ears as opposed to a pair of independent ears. We will also have an idea about the frequency regimes that correspond to the use of iTDs and iLDs in localization.

3.1 Sound Localization Using the ICE–Model

In our study we are primarily concerned with hearing in geckos. We will be using parameters (interaural separation, tympanum area etc.) from *Hemidactylus frenatus*, the common house gecko [16] and the Tokay gecko [4], [17]. In order to proceed with our evaluation of our model, we will need to assign appropriate numerical values to the parameters we have defined in 2.1. For now we will simply list the values and leave the discussion to a later point.

Table 3.1: ICE Model geometry Parameters for the common house gecko (*Hemidactylus frenatus*) and the Tokay gecko.

Parameter name	Hemidactylus	Tokay gecko
Length of the cylinder or interaural distance, L	10mm	22mm
Radius of the tympanic membrane, a_{tym}	1.5mm	2.6mm
Fundamental frequency (first eigenfrequency) of the tympanic membrane, ω_{01}	3200Hz	1050Hz
Quality factor of the tympanum, Q	1.3	1.4
Density of the membrane material, ρ_m	1mg/mm ³	1mg/mm ³
Thickness of the membrane, d	8μm	10μm
Volume of the cavity, V_{cav}	.32ml	3.5ml
Extracolumella angle, β	π/25	π/25
Cylinder radius calculated from V_{cav} and L using the formula given in (2.1), a_{cyl}	~ 6.6mm	~ 3.2mm

From these quantities it should be apparent that the house gecko, with an interaural separation of 10mm and mouth cavity volume of .32ml is a rather small lizard. The Tokay gecko is the second largest gecko species (interaural separation of 22mm and mouth cavity volume 3.5ml, [16]). Thus we will demonstrate the scalability of our model with regards to hearing in animals with widely varying head widths and mouth cavities. As we will subsequently see, the geometric parameters, especially the head width and the membrane eigenfrequencies, put important limits on the “hearing range” of our model.

Before we begin our comparison of the data, we should first acquaint ourselves with some experimental details. As already mentioned in Sec. 2.1.3, the geckos were placed in an anechoic room. They were subject to 175ms frequency sweeps (200-7500 Hz) at levels of 80-90 dB with the speakers placed at a 1m distance. The eardrum vibrations were then measured using laser-Doppler vibrometry with the point of measurement at the tip of the extracolumella. The measured values correspond to the displacement velocity of the membrane at this point. In our analysis, the point corresponding to the tip of the extracolumella is stationary and cannot be used to compare the vibrations of the

membranes. Instead, we use the total membrane displacements defined in the previous chapter which are given by,

$$S^0 = G_{ipsi}^s p_0 + G_{contra}^s p_L \quad (3.1)$$

$$S^L = G_{ipsi}^s p_L + G_{contra}^s p_0 \quad (3.2)$$

$$\dot{S}^{0/L} = j\omega S^{0/L} \quad (3.3)$$

using the ipsi- and contralateral filters for the total displacement defined in (2.63) and (2.64). The definition of the total membrane velocity given in the second line follows directly from the definition of the membrane displacements. Following Sec. 2.1.3 and (2.2), the sound pressure inputs have the form

$$p_0 = p e^{j\omega t} e^{j\Delta_{new}/2}, \quad p_L = p e^{j\omega t} e^{-j\Delta_{new}/2}, \quad \Delta_{new} = 1.5kL \sin \theta. \quad (3.4)$$

The rest of this section follows from the above definitions. In Sec. 3.1.1 we study the dependence of the membrane vibration velocity on the frequency and direction of the sound source. Using the membrane vibration velocity we will define the main directional hearing cues - the Internal Time and Level Differences - in Sec. 3.1.2. As mentioned earlier, we will conclude by justifying our selection of parameters. In Sec. 3.1.3 we will analyse the dependence of the expressions defined in previous sections on the system parameters and in this way also provide estimates for realistic material parameters.

3.1.1 Membrane Vibration Velocity

We will first evaluate the variation of the membrane displacements with respect to external sound stimuli. Before we begin, we should note that although the quantities $\dot{S}^{0/L}$ will not quantitatively reproduce the experimentally measured membrane vibrations, their behaviour with respect to frequency and direction is consistent. They also have the added advantage that they only depend on direction and frequency. In Fig. 3.1, we compare the normalized velocity of the tympanic membrane ($\dot{S}^{0/L}/(\pi a_{cyl}^2)$) with the membrane velocity measured using laser vibrometry in [4] and [16]. The plot shows the vibration amplitude as a function of frequency (y -axis) and direction (x -axis). The amplitudes are given in units of dB re 1 mm/(s Pa). This means that we have plotted the ratio vibration amplitude with reference to a vibration velocity of 1 mm/s with an input pressure of 1 Pa. In other words we have set $p = 1 \text{ Pa}$ in (3.4).

As we can see, the total membrane velocities reproduce the frequency and direction dependence of the system fairly well. The directional behaviour is consistent with regard to the requirement that the membrane have a higher vibration amplitude when it is on the same side as the object. The reason for the deviation from experimental behaviour at higher frequencies isn't currently known. The mechanics of the extracolumella including its flexion and the influence of the realistic shape of the mouth cavity could offer possible explanations. Although the room was tested to be anechoic to below 200Hz some reflections, especially from the laser setup are unavoidable. This is the cause of the spectral ripple in

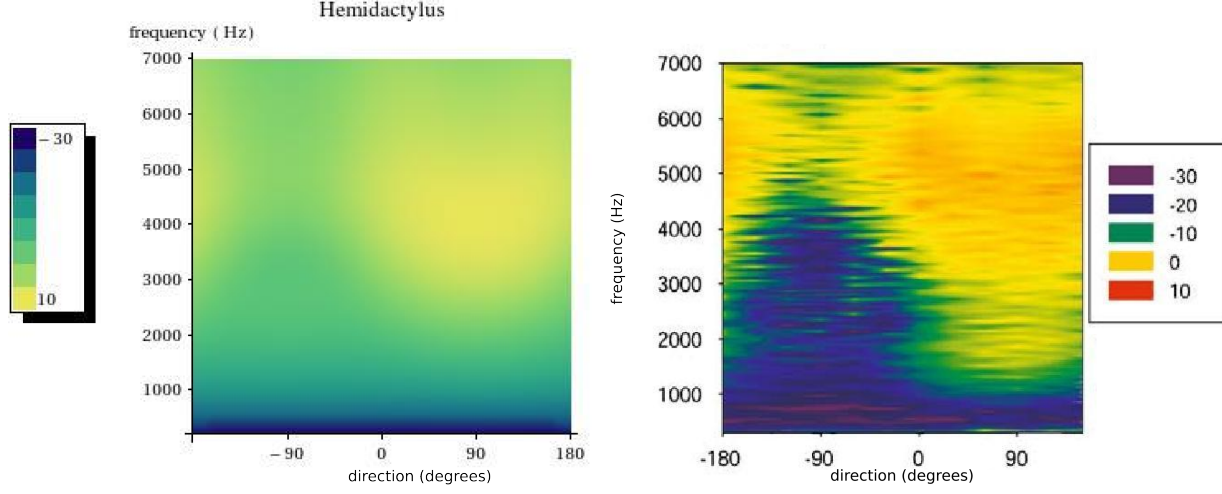


Figure 3.1: Calculated (left) and experimental (right) amplitude of tympanic membrane vibrations for *Hemidactylus frenatus* in dB re 1 mm/(s Pa), i.e. the ratio of the vibration amplitude with reference to a vibration velocity of 1 mm/s with an input pressure of 1 Pa. On the x -axis we have the direction of the sound source in degrees varying from -180° to 180° with positive angles corresponding to ipsilateral stimuli. The legends on the left and right denote the amplitude in decibels. The calculate values are from the ICE model and the experimental values are taken from Christensen-Dalsgaard [16].

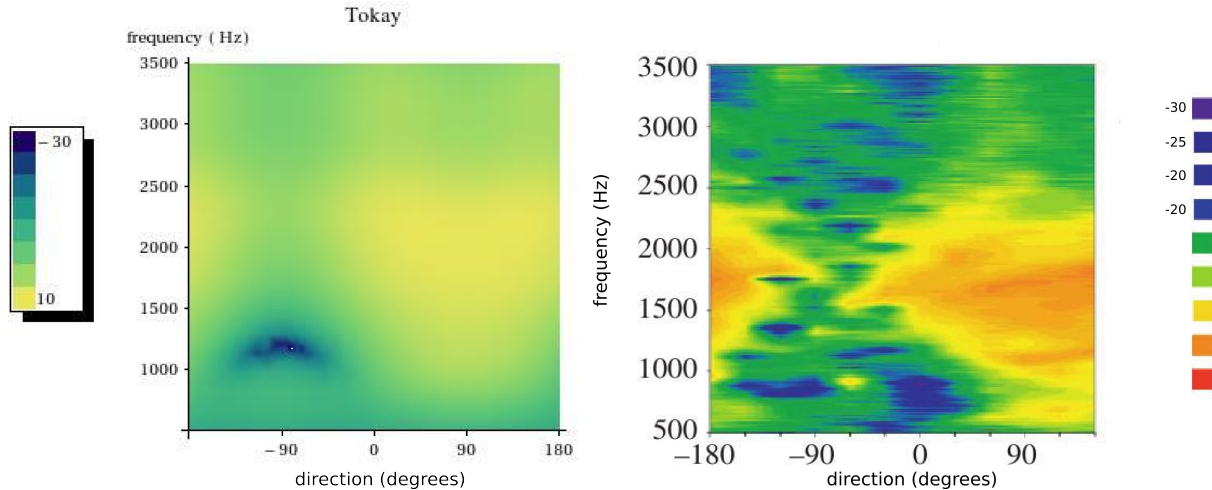


Figure 3.2: Calculated (left) and experimental (right) amplitude of tympanic membrane vibrations for the Tokay gecko in dB re 1 mm/(s Pa). The axis and legend values are the same as the ones in Fig. 3.1. The experimental values are taken from Christensen-Dalsgaard [4].

the experimental measurements. The same comparison is illustrated for the Tokay gecko in Fig. 3.2 (data from [4]).

In order to get a better understanding of the directionality of the model, it is also important to look at the dependence of the vibration amplitudes on direction and frequency independently. In Fig. 3.3 (house gecko) and Fig. 3.4 (Tokay gecko) we have plotted the membrane vibration velocity for a pure ipsilateral stimulus (90°) and pure contralateral stimulus (-90°) as a function of frequency. As we can see the ipsilateral response is generally

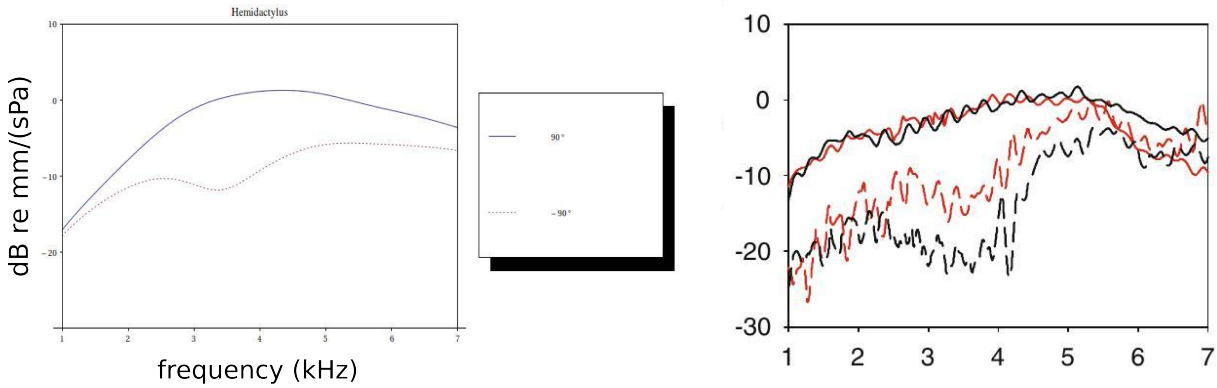


Figure 3.3: Calculated (left) and experimental (right) vibration velocity spectra for the common house gecko. The two plots on the left correspond to the response of the tympanic membrane to a purely ipsilateral (90°) and purely contralateral (-90°) stimulus. The two colours on the right correspond to different individuals of the house gecko species. Experimental values taken from Christensen-Dalsgaard [16].

higher than the contralateral response and the difference peaks at a certain frequency i.e., it has a bandpass characteristic which is consistent with observations. These amplitude differences can be used to localize the sound source; see Sec. 3.1.2. At very low and very high frequencies the both the vibration amplitudes converge. In Fig. 3.5 we have also plotted the response of the ear to ipsi- and contralateral stimuli with varying directions. ($90^\circ, 60^\circ, 0^\circ, -60^\circ, -90^\circ$) and thereby shown that the vibration amplitude is higher when the sound source is nearer to the ear (i.e. θ is closer to 90°).

We conclude this section by looking at the directional dependence of the vibration for a given set of frequencies. In Fig. 3.6, we show the variation of the vibration amplitude of the membrane as the sound source moves around the animal i.e. as θ varies from -180° to 180° . Here we can more clearly see that the amplitudes due to ipsilateral stimuli are higher than those due to contralateral stimuli. The marked asymmetry and the steepness across the midline (i.e. at 0°) is also consistent with observations ([4], [16]). The choice of our frequencies has to do with the typical hearing ranges of the geckos. The smaller house gecko is most sensitive at higher frequencies (3kHz) and the larger Tokay gecko at lower frequencies (1kHz).

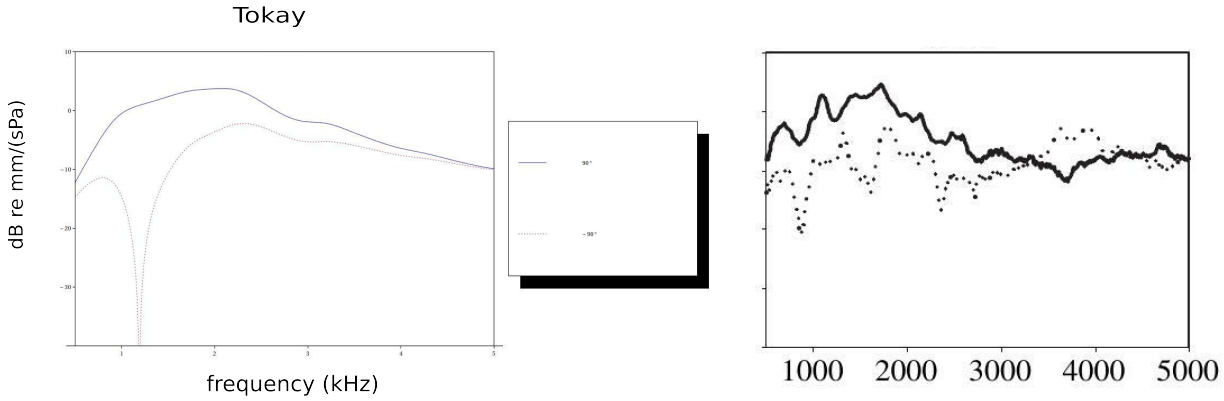


Figure 3.4: Calculated (left) and experimental (right) vibration velocity spectra for the Tokay gecko. In the plot on the right hand side, the thick line corresponds to an ipsilateral stimulus and the dotted line to a contralateral stimulus. Data from [4].

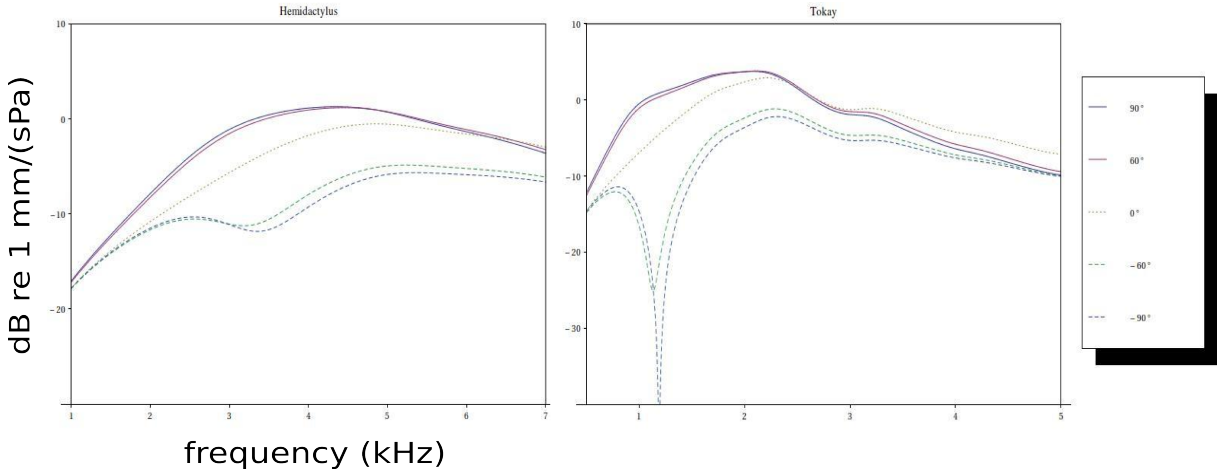


Figure 3.5: Frequency dependence of membrane vibration amplitudes for different directions - common house gecko (left), Tokay gecko (right). The amplitude response to ipsilateral stimuli is generally higher and is at a maximum when the object is nearest to the ear i.e. $\theta = 90^\circ$. The dotted line denotes a sound source directly in front of or behind the animal and the dashed lines denote contralateral stimuli.

3.1.2 Directional Hearing Cues

The significance of our results upto this point should already be apparent. Due to the relatively small head sizes of the geckos, the sound arriving at the two ears differ very slightly in phase and not at all in amplitude. On the other hand these animals overcome the problem and create strongly directional membrane vibration amplitudes through the use of coupled ears. From form of the direction dependence of the membrane vibration amplitudes we see that individual amplitudes don't necessarily vary much with direction. In other words, although there is a clear difference between the ipsilateral and contralat-

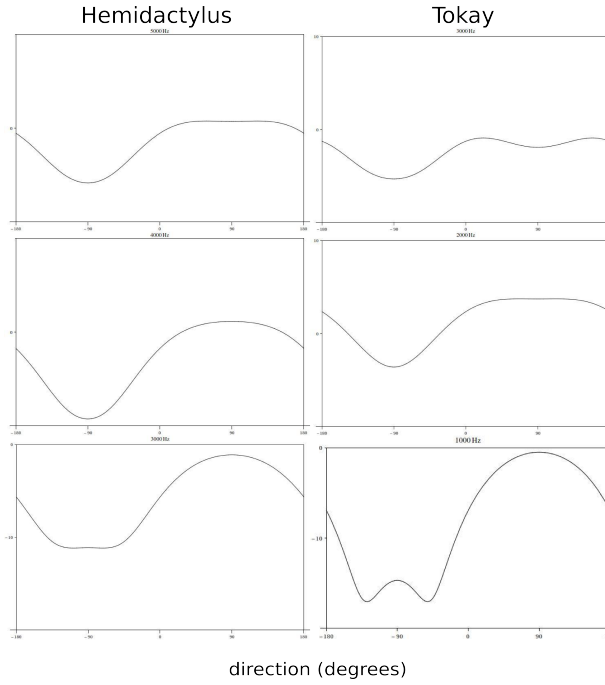


Figure 3.6: Direction dependence of membrane vibration amplitudes in the ICE Model for different frequencies - common house gecko (left, at 3kHz, 4kHz and 5kHz), Tokay gecko (right, at 1kHz, 2kHz and 3kHz). The variation of the amplitude as the sound source completes a full circle around the animal is illustrated. The amplitudes for ipsilateral stimuli are shown to be higher than those for contralateral stimuli.

eral response, the difference between a given pair of ipsi- or contralateral directions (eg. between 90° and 75° or between -90° and -70°) isn't very significant. Moreover, for some frequencies it seems that the vibration amplitude is lower at $\theta = 90^\circ$ than at $\theta \sim 60^\circ$. As a result of this, the vibration amplitudes of the ears cannot be independently used to localize the objects. In order to do so by using the tympanic membrane vibration amplitudes, we need to compare the variation of their differences with respect to direction. We therefore need functions that accurately quantify the directional dependence of the system at a given frequency.

As a first step we define the two quantities that are the main focus of this chapter - the internal level difference (iLD) and internal time difference (iTID) in terms of the total membrane velocities.

$$\text{iLD} := 20\text{Log}_{10} \left(\left| \frac{\dot{S}^0}{\dot{S}^L} \right| \right) \quad (3.5)$$

$$\text{iTD} := \text{Arg} \left(\frac{\dot{S}^0}{\dot{S}^L} \right) / \omega. \quad (3.6)$$

Due to the steady state approximation we have the added advantage that the ratio of the displacement amplitudes is equal to that of the velocity amplitudes; see (2.31). The main

advantage of the velocity amplitudes is their relative ease of measurement in experiments. The iLD measures the ratio between the amplitudes of the eardrums and is the same as the IVAD function defined by Jørgensen *et al.* [27] and is measured in dB. The iLD is positive for ipsilateral directions and negative for contralateral. This agrees with observed behaviour and means that the response of the system is directional. The iTD corresponds to the time difference (or equivalently phase difference) between the membrane vibrations. The ipsilateral ear is always ahead in phase with respect to the contralateral ear. This means that it is negative for ipsilateral directions and positive for contralateral.

The iTD and iLD can be seen as the output of the ICE system with p_0 and p_L as inputs. In contrast, the Interaural Time and Level Differences (ITD and ILD) are entirely determined by the inputs to the two ears. The ITD is defined as the time sound takes to travel across the head width and is given by $\text{ITD} = L/c$. It is equivalent to Δ , the phase difference between the vibrations of the eardrums without coupling and diffraction effects; see (2.2). Due to the input pressures having the same amplitude and due to the linearity of the system (w.r.t sound input), the ICE model does not have any a priori Interaural Level Difference. In larger animals like humans the difference between the input amplitudes increases with frequency due to diffraction effects (shadowing) which aids in localization; cf. [26, p .154]. In addition, the gain in ITD due to their increased head size also provides sufficient information for localization at lower frequencies.

In order to effectively function as cues for localization the iLDs and iTDs should ideally satisfy the following requirements,

1. For a significant frequency range, they should increase with the adjacency of the sound source and should reach their maximum at $\theta = 90^\circ$ and their minimum at $\theta = -90^\circ$.
2. The iTD in particular should remain more or less constant for a given frequency range thereby mirroring the behaviour of the ITD. This is advantageous from the point of view of neuronal processing.
3. They should go to zero at $\theta = 0^\circ$ and $\theta = \pm 180^\circ$ meaning they should vanish when the object is directly in front of and behind the animal.

The last of these requirements is ensured by the symmetry of our system as $p_0 = p_L$ at $\theta = 0^\circ$ and $\pm 180^\circ$. The first and second, on the other hand are more subtle aren't necessarily satisfied for all systems but we will subsequently see, with our choice of parameters they will be to a great degree. In Fig. 3.7 (house gecko) and Fig. 3.8, we plot the variation of the iLD with direction and frequency. The conventions for the x - and y -axes remain the same as the ones in Figures 3.1 and 3.2. The iLDs vary systematically with frequencies and peaks at around 3kHz for the house gecko and around 1kHz for the Tokay gecko. As expected, they are positive for ipsilateral directions and negative for contralateral.

The contour plots serve the purpose of giving us the simultaneous frequency and direction dependence of the iLDs well but the satisfaction of first requirement given in above list isn't automatically clear. In Fig. 3.9 we plot the variation of iLDs with direction for

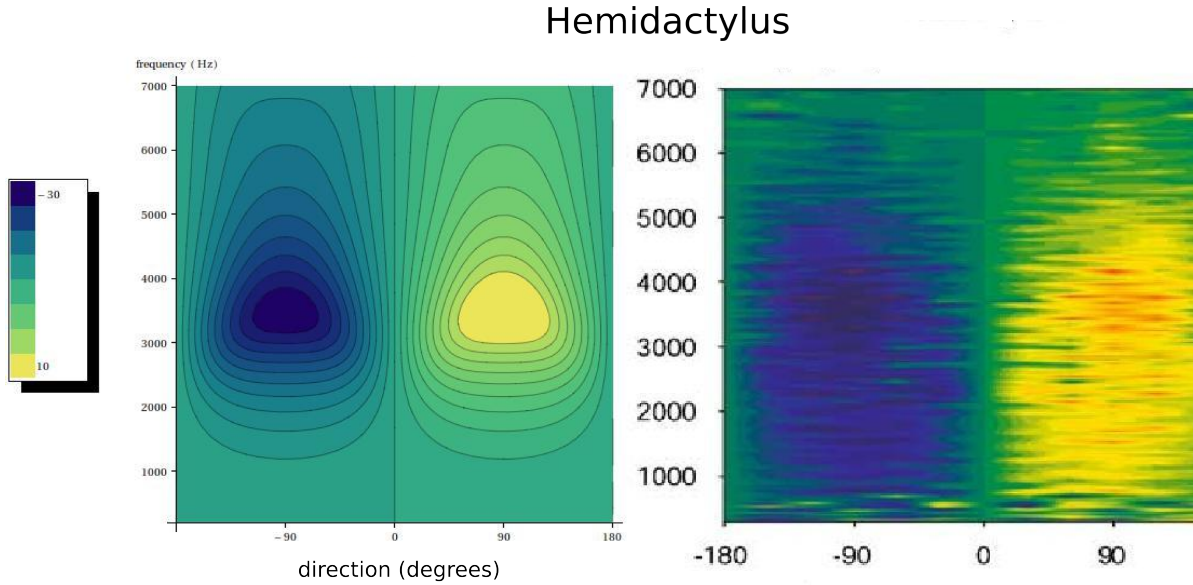


Figure 3.7: Calculated (left) and experimental (right) Internal Level Difference of tympanic membrane vibrations for the common house gecko in dB. x -axis denotes direction in degrees (negative angles contralateral, 0 frontal and positive angles ipsilateral and the y -axis frequency in kHz. Calculated and experimental values [16] show similar qualitative behaviour. See also Fig. 3.8.

a given set of frequencies for the house gecko (left) and Tokay gecko (right). We see that although the iLD has higher values at 1kHz, the form of the iLD for higher frequencies reflects the sinusoidal input better by peaking at fully ipsilateral and contralateral directions. This suggests that iLDs may work better as directional cues at higher frequencies.

3.1.3 Parameter Estimation

Upto this point we have calculated the desired quantities in our model by using the values given in Table 2.1. Some of the parameters can be directly taken from their measured values whereas the rest will need to be estimated indirectly. For the head width/interaural distance (L), cavity volume (V_{cav}), the density of the membrane (ρ_m)¹ and its thickness (d) we can use the directly measured values. The radius of the cylinder (a_{cyl}) can be calculated from the first two quantities using (2.1). As we've already seen in Fig. 2.4, the realistic tympanic membrane is an ellipsoid rather than a perfect circle therefore the radius of our tympanum will instead be estimated from the area of the membrane as $a_{tym} = \sqrt{A/\pi}$. For the extracolumella angle (β), we use the value estimated by Vossen [13].

¹A caveat: The density given in common models for the tympanum is around 3mg/mm^3 but this includes the mass of the transducer (the extracolumell). The density of the material of the tympanic membrane is in fact closer to the density of water, hence the chosen value of 1mg/mm^3

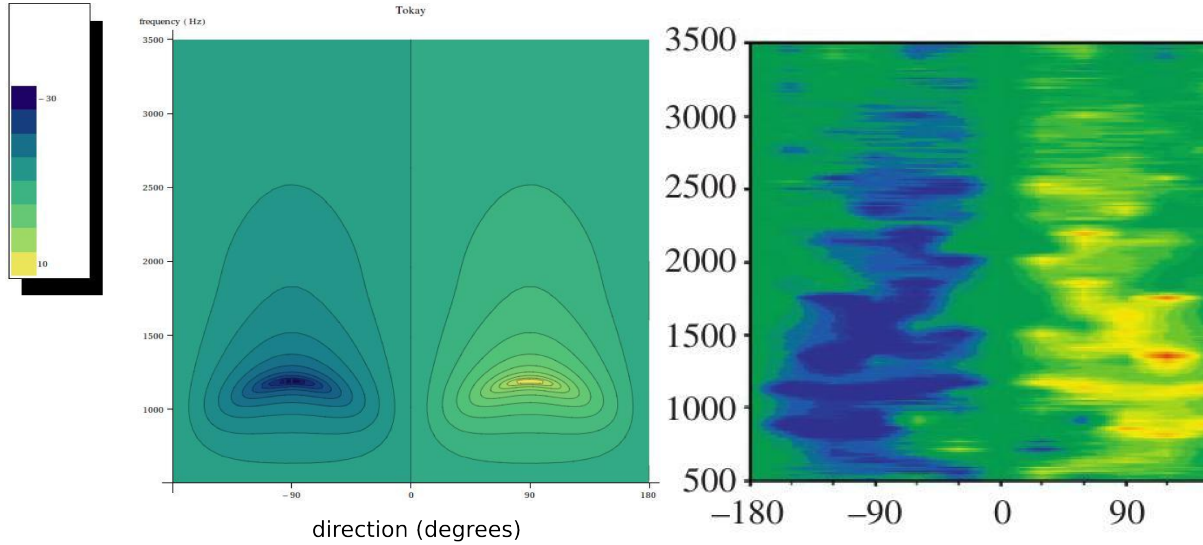


Figure 3.8: Calculated (left) and experimental (right) Internal Level Difference of tympanic membrane vibrations for the Tokay gecko in dB. The experimental values are taken from Christensen-Dalsgaard [4].

The parameters that require an indirect estimation are the first membrane eigenfrequency (ω_{01}) and its quality factor Q . The first of these effectively gives us the propagation speed of membrane vibrations, $c_M = \omega_{01}/\mu_{01}$ and the second gives us the membrane damping, $\alpha = \omega_{01}/2Q$. These quantities are difficult to directly measure and instead have to be estimated from the frequency response of the system.

A hint for the approximate values of ω_{01} and α comes from the bandpass nature of the Internal Level Differences and the frequency at which the iLD maximum is attained. This suggests that one of the membrane eigenmodes is dominant. In addition, as we have already seen, the iTDs remain constant for a significant frequency range ([17, p .1996]) putting further constraints on the value of α . For the house gecko they have been experimentally is around 3kHz and around 1.4kHz for the Tokay gecko. Due to the complexity of the expression for the membrane vibration profile, the exact position of the iLD maximum is hard to directly calculate. In order to better understand our parametre selection, we need to take a closer look at the analytical expression for the displacement ratio of the membranes,

$$\frac{\dot{S}^0}{\dot{S}^L} = \frac{\eta + e^{1.5jkL \sin \theta}}{1 + \eta e^{1.5jkL \sin \theta}} \quad (3.7)$$

where, $\eta = \frac{G_{ipsi}^s}{G_{contra}^s} = \frac{\Lambda}{\rho c \omega} \sin kL - \cos kL$.

We have simplified the above expression after using the appropriate formulas for G_{ipsi}^s

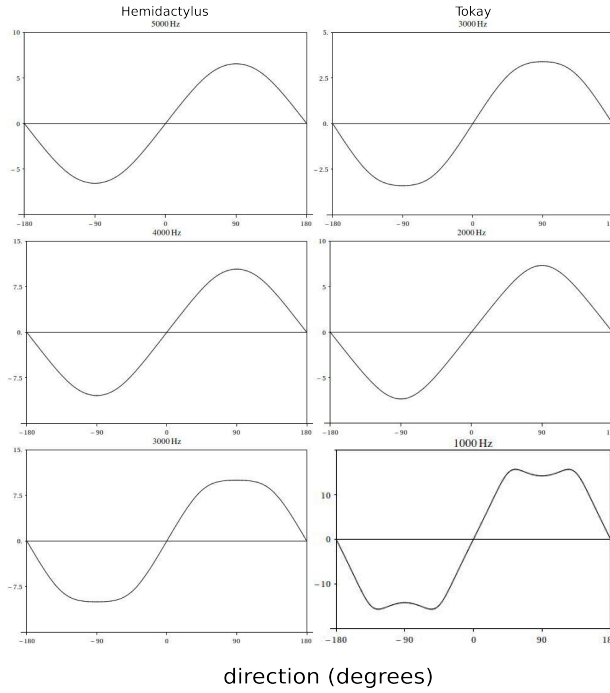


Figure 3.9: Direction dependence of the the Interaural Level Difference (cf. (3.5)) in the ICE Model for different frequencies - common house gecko (left, at 3kHz, 4kHz and 5kHz) , Tokay gecko (right, at 1kHz, 2kHz and 3kHz). At higher frequencies, the iLD reaches a maximum at 90° and a minimum at -90° whereas for lower frequencies, the maxima and minima are reached before and after. This form of the above plots suggests that the iLD work better as directional cues at higher frequencies.

and G_{contra}^s . We now set the direction of the source to be fully ipsilateral to the $x = 0$ membrane, i.e. 90° . The complex frequency dependence of the above term is entirely contained in the term η . As stated towards the end of Sec. 2.2.3, we have to choose an appropriate cutoff for the value of Λ . This choice is itself dependent on the values of ω_{01} and α and therefore on the specific animal. It is further complicated by the fact that the corresponding zeros of the Bessel function J_κ are very closely spaced.

3.2 Spatial Vibration Pattern of the Membrane

We begin our analysis by evaluating the variation of the spatial vibration pattern of the tympanic membrane with frequency. The tympanic vibration pattern was first measured experimentally by Manley [15] for a *Tokay gecko* and was found to have the strongest response at around 1kHz. The measured vibration patterns are shown on the left in Fig. 3.10. Manley measured the vibration amplitude for eight locations on the membrane and measured the pattern seen on the left of Fig. 3.10. As we can see, at around 4kHz, the vibration pattern distinctly develops two maxima - something that would not happen to a centrally loaded tympanum except at frequencies well beyond the hearing range of geckos.

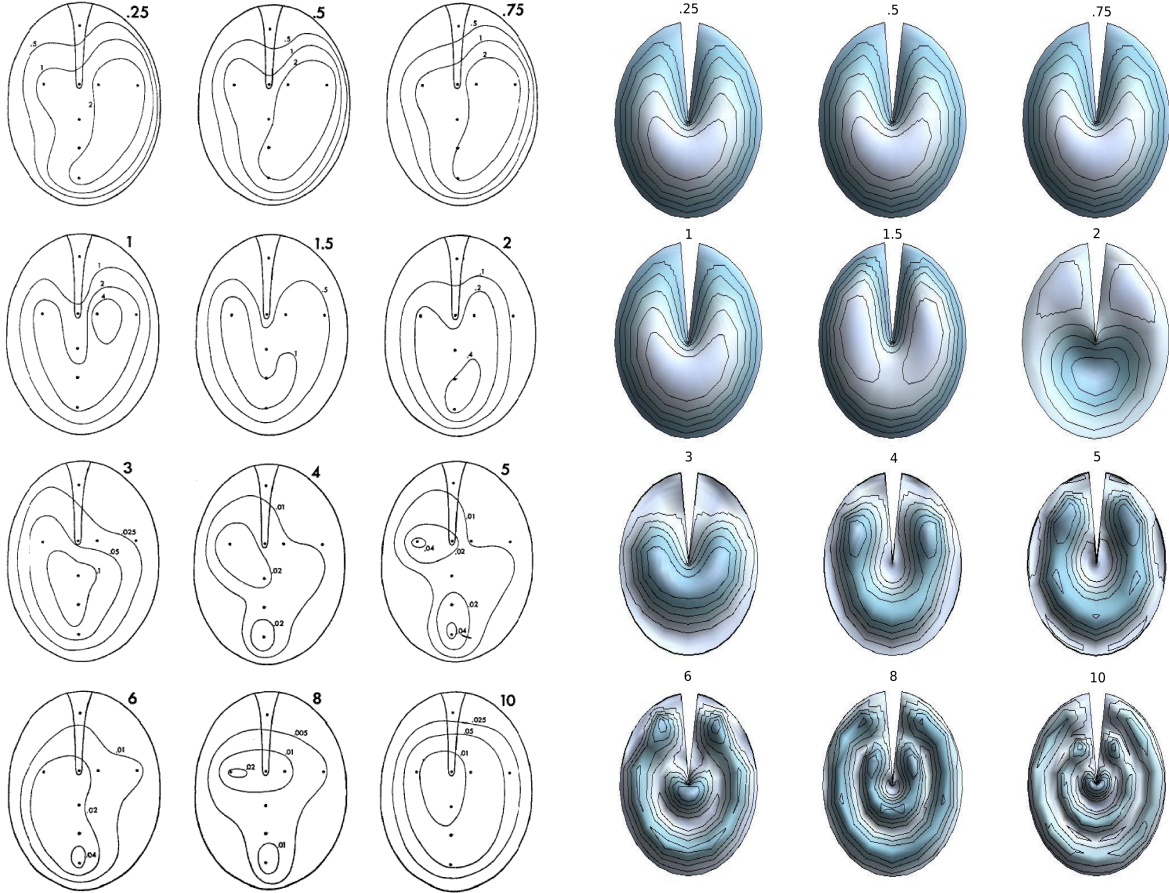


Figure 3.10: Experimental membrane vibration patterns of the Tokay gecko dependent on sound frequency varying from .5kHz to 10kHz. Data taken from [15].

In order to compare our model with the experimental results, we plot the response of one of the membranes ($x = 0$, although $x = L$ could be chosen equivalently due to the symmetry of the system) in our cylindrical ICE model calculated using (2.59). The opposite ear was chosen to be blocked, meaning $p_L = 0$. This is illustrated in Fig. 3.10 (right) for the same frequency range as in the experimental data. The sound pressure input was chosen to have unit amplitude and the model parameters used are given on the right most column of Table 3.1. The omitted region corresponds to the extracolumella.

The asymmetric nature of our membrane vibration pattern is a result of our chosen geometry. Mathematically this is a result of the fact that a uniform pressure (on the membrane surface) on a full circular membrane only couples to the circularly symmetric J_0 modes. In the case of the sectoral membrane however, the uniform pressure couples to all the eigenmodes resulting in a more complex pattern. As a qualitative reproduction our model is very accurate but for a full quantitative analysis, we would need to account

for the motion of the extracolumnella. Moreover, the full mechanics of the extracolumnella including its flection at higher frequencies can have significant effects which have not been studied so far.

Chapter 4

Conclusion

Bibliography

- [1] C. E. Carr, D. Soares, J. Smolders, and J. Z. Simon, “Detection of interaural time differences in the alligator,” *J. Neurosci.*, vol. 29, pp. 7978–7990, Jun 2009.
- [2] J. Christensen-Dalsgaard and C. Carr, “Evolution of a sensory novelty: tympanic ears and the associated neural processing.,” *Brain Res Bull*, vol. 75, no. 2-4, pp. 365–70, 2008.
- [3] J. W. Schnupp and C. E. Carr, “On hearing with more than one ear: lessons from evolution,” *Nature Neuroscience*, vol. 12, pp. 692–697, jun 2009.
- [4] J. Christensen-Dalsgaard and G. A. Manley, “Directionality of the lizard ear,” *J. Exp. Biol.*, vol. 208, pp. 1209–1217, Mar 2005.
- [5] A. Michelsen, “Hearing and sound communication in small animals: Evolutionary adaptations to the laws of physics,” in *The Evolutionary Biology of Hearing* (D. Webster, A. Popper, and R. Fay, eds.), pp. 61–77, Springer New York, 1992.
- [6] H. Autrum, “Über lautäußerungen und schallwahrnehmung bei anthropoden ii.,” *Journal of Comparative Physiology*, vol. 28, pp. 326–352, 1940.
- [7] A. Michelsen and O. N. Larsen, “Pressure difference receiving ears,” *Bioinspiration & Biomimetics*, vol. 3, no. 1, p. 011001, 2008.
- [8] H. F. Olson, “Gradient microphones,” *The Journal of the Acoustical Society of America*, vol. 17, no. 3, pp. 192–198, 1946.
- [9] D. Robert, R. Miles, and R. Hoy, “Directional hearing by mechanical coupling in the parasitoid fly *ormia ochracea*,” *Journal of Comparative Physiology A*, vol. 179, no. 1, pp. 29–44, 1996.
- [10] A. Michelsen, “Biophysics of sound localization in insects,” in *Comparative Hearing: Insects* (R. Hoy, A. Popper, and R. Fay, eds.), vol. 10 of *Springer Handbook of Auditory Research*, pp. 18–62, Springer New York, 1998.
- [11] M. Jrgensen, “Comparative studies of the biophysics of directional hearing in anurans,” *Journal of Comparative Physiology A*, vol. 169, no. 5, pp. 591–598, 1991.

- [12] C. Voßen, *Auditory Information Processing in Systems with Internally Coupled Ears*. PhD thesis, Technische Universität München, 2010.
- [13] C. Voßen, J. Christensen-Dalsgaard, and J. L. van Hemmen, “Analytical model of internally coupled ears.,” *Journal of the Acoustical Society of America*, vol. 128, pp. 909–918, 2010.
- [14] G. Manley, “Frequency response of the middle ear of geckos,” *Journal of comparative physiology*, vol. 81, no. 3, pp. 251–258, 1972.
- [15] G. A. Manley, “The middle ear of the tokay gecko,” *Journal of Comparative Physiology*, vol. 81, no. 3, pp. 239–250, 1972.
- [16] J. Christensen-Dalsgaard and G. Manley, “Acoustical coupling of lizard eardrums,” *Journal of the Association for Research in Otolaryngology*, vol. 9, no. 4, pp. 407–416, 2008.
- [17] J. Christensen-Dalsgaard, Y. Tang, and C. E. Carr, “Binaural processing by the gecko auditory periphery,” *J. Neurophysiol.*, vol. 105, pp. 1992–2004, May 2011.
- [18] C. Köppl and C. Carr, “Maps of interaural time difference in the chickens brainstem nucleus laminaris,” *Biological Cybernetics*, vol. 98, no. 6, pp. 541–559, 2008.
- [19] L. Rayleigh and A. Lodge, “On the acoustic shadow of a sphere. with an appendix, giving the values of legendre’s functions from p0 to p20 at intervals of 5 degrees,” *Philosophical Transactions of the Royal Society of London. Series A, Containing Papers of a Mathematical or Physical Character*, vol. 203, pp. pp. 87–110, 1904.
- [20] L. Rayleigh, *Theory of Sound: V. 1*. Dover Publications., 1900.
- [21] S. Rschevkin, O. Blunn, and P. Doak, *A Course OF Lectures On Sound*. Pergamon, 1963.
- [22] S. Temkin, *Elements of Acoustics*. Wiley, 1981.
- [23] E. T. Copson, *Introduction to the Theory of Functions of a Complex Variable*. Oxford: Clarendon Press, 1973.
- [24] C. Pozrikidis, *Fluid Dynamics: Theory, Computation, and Numerical Simulation*. Springer, 2009.
- [25] N. Asmar, *Partial Differential Equations with Fourier Series and Boundary Value Problems*. Pearson Education, Limited, 2005.
- [26] N. H. Fletcher, *Acoustic Systems in Biology*. Oxford: Oxford University Press, 1992.
- [27] M. Jørgensen, B. Schmitz, and J. Christensen-Dalsgaard, “Biophysics of directional hearing in the frog eleutherodactylus coqui,” *Journal of Comparative Physiology A*, vol. 168, no. 2, pp. 223–232, 1991.

Acknowledgements

Danke.